

1
2
3
4
5
6
7
8
9
10
11
12
13
14
15
16
17
18
19
20
21
22
23
24
25
26
27

Manuscript prepared for Geosci. Model Dev.

Date: 10 May 2018

PCR-GLOBWB 2: a 5 arc-minute global hydrological and water resources model

Edwin H. Sutanudjaja¹, Rens van Beek¹, Niko Wanders¹, Yoshihide Wada^{1,2}, Joyce H.C. Bosmans¹, Niels Drost³, Ruud J. van der Ent¹, Inge E. M. de Graaf⁴, Jannis M. Hoch^{1,5}, Kor de Jong¹, Derek Karssenberg¹, Patricia López López^{1,5}, Stefanie Peßenteiner⁶, Oliver Schmitz¹, Menno W. Straatsma¹, Ekkamol Vannamete⁷, Dominik Wisser⁸, and Marc F. P. Bierkens^{1,9}

- 1 Department of Physical Geography, Faculty of Geosciences, Utrecht University, Utrecht, The Netherlands
- 2 International Institute for Applied Systems Analysis, Laxenburg, Austria
- 3 Netherlands eScience Center, Amsterdam, The Netherlands
- 4 Chair of Environmental Hydrological Systems, University of Freiburg, Freiburg, Germany,
- 5 Unit Inland Water Systems, Deltares, Delft, the Netherlands
- 6 Department of Geography and Regional Science, University of Graz, Graz, Austria
- 7 Department of Geography, Chulalongkorn University, Bangkok, Thailand
- 8 Center for Development Research, University of Bonn, Bonn, Germany
- 9 Unit Soil and Groundwater Systems, Deltares, Utrecht, The Netherlands

Correspondence to: E. H. Sutanudjaja (E.H.Sutanudjaja@uu.nl)

28

29 **Abstract**

30

31 We present PCR-GLOBWB 2, a global hydrology and water resources model. Compared to previous versions of
32 PCR-GLOBWB, this version fully integrates water use. Sector-specific water demand, groundwater and surface
33 water withdrawal, water consumption and return flows are dynamically calculated at every time step and interact
34 directly with the simulated hydrology. PCR-GLOBWB 2 has been fully rewritten in Python and PCRaster-Python
35 and has a modular structure, allowing easier replacement, maintenance, and development of model components.
36 PCR-GLOBWB 2 has been implemented at 5 arc-minute resolution, but a version parameterized at 30 arc-minute
37 resolution is also available. Both versions are available as open source codes on [https://github.com/UU-](https://github.com/UU-Hydro/PCR-GLOBWB_model)
38 [Hydro/PCR-GLOBWB_model](https://github.com/UU-Hydro/PCR-GLOBWB_model). PCR-GLOBWB 2 has its own routines for groundwater dynamics and surface
39 water routing. These relatively simple routines can alternatively be replaced by dynamically coupling PCR-
40 GLOBWB 2 to a global two-layer groundwater model and 1D-2D-hydrodynamic models, respectively. Here, we
41 describe the main components of the model, compare results of the 30 arc-minute and the 5 arc-minute versions
42 and evaluate their model performance using GRDC discharge data. Results show that model performance of the 5
43 arc-minute version is notably better than that of the 30 arc-minute version. Furthermore, we compare simulated
44 time series of total water storage (TWS) of the 5 arc-minute model with those observed with GRACE, showing
45 similar negative trends in areas of prevalent groundwater depletion. Also, we find that simulated total water
46 withdrawal, matches reasonably well with reported water withdrawal from AQUASTAT, while water withdrawal
47 by source and sector provide mixed results.

48

49

50 **1 Introduction**

51

52 The last decades saw the development of an increasing number of global hydrological models (GHMs), e.g. VIC
53 (Liang et al., 1994, Nijssen et al., 2001), WMB (Fekete et al., 2002), WaterGAP (Döll et al., 2003), H08 (Hanasaki
54 et al., 2008a, Hanasaki et al., 2018), MAC-PDM (Gosling and Arnell, 2011) (see Bierkens et al., 2014, Bierkens,
55 2015 and Kauffeldt et al. 2016 for a more extensive list, also including land surface models). GHMs have become
56 essential tools to quantify and understand the global terrestrial water cycle, as they simulate the distributed
57 hydrological response to weather and climate variations at higher resolution (typically $0.5^{\circ}\times 0.5^{\circ}$) than used
58 previously in general circulation models (GCMs), with more sophisticated runoff generation processes and river
59 routing. As such, global hydrological models have been used for medium-range to seasonal flood forecasting
60 (Bierkens and van Beek, 2009, Alfieri et al., 2013, Candogan Yossef et al., 2013) as well as for a myriad of water-
61 related global change assessments. Examples are: the projection or estimation of future flood and drought events
62 (Sperna-Weiland et al., 2012, Dankers et al., 2013, Prudhomme et al., 2013, Wanders et al. 2015, Wanders and
63 Wada, 2016), current and future flood hazard and risk (Pappenberger et al., 2012, Hirabayashi et al., 2013, Ward et
64 al., 2013, Winsemius et al., 2013, 2016), global groundwater depletion (Wada et al., 2010, Gleeson et al., 2012),
65 the contribution of terrestrial water stores to global sea level change (Konikow, 2011, Wada et al., 2012, Pohkrel et
66 al., 2013), current and future water scarcity under climate change and increasing population growth (Hanasaki et
67 al., 2008b, Wada et al., 2011a, 2011b, Schewe et al., 2014, Haddeland et al., 2014, Wada and Bierkens, 2014), tele-
68 connections between climate oscillations and water availability (Wanders and Wada, 2015), the impact of land use
69 change on global water resources (Rost et al., 2008, Sterling et al., 2015, Bosmans et al., 2017) and trends in
70 surface water temperature and cooling water potential (van Beek et al., 2012, van Vliet et al., 2012). More recently,
71 the output from global hydrological models has been extended to study socioeconomic impacts, such as virtual
72 water trade (Konar et al., 2013, Dalin et al., 2017) and future agricultural production (Elliott et al., 2013). These
73 applications show that GHMs have become invaluable tools in support of global change research and
74 environmental assessments.

75

76 PCR-GLOBWB (PCRaster GLOBAL Water Balance) (van Beek and Bierkens, 2009, van Beek et al. 2011) is one of
77 the recently developed GHMs. PCR-GLOBWB is a grid-based global hydrological model developed at the
78 Department of Physical Geography, Faculty of Geosciences, Utrecht University, the Netherlands. The model,
79 describing the terrestrial part of the hydrological cycle, was first introduced in a technical report by van Beek and
80 Bierkens (2009) and then formally published in a paper of van Beek et al. (2011), focusing on global water
81 availability issues. PCR-GLOBWB was originally developed to solve the global daily surface water balance with a
82 spatial resolution of 30 arc-minutes (about 50 km by 50 km at the equator) and compare the resulting fresh water
83 availability with monthly sectoral water demand in order to assess global-scale water scarcity (van Beek et al.,
84 2011, Wada et al., 2011a,b). In this first version of PCR-GLOBWB (called PCR-GLOBWB 1 hereafter), similar to
85 other global-scale hydrological models, water demand and water availability are treated independently, i.e. without
86 direct feedback between human water use and other terrestrial water fluxes (e.g. Döll and Siebert, 2002, Wisser et

87 al., 2010). Since it was first introduced, PCR-GLOBWB has been applied extensively in global water resources
88 assessment studies. For instance, a recent search on Scopus (accessed on 13 April 2018) on the key-word “PCR-
89 GLOBWB” yielded 113 publications with collectively over 2500 citations. Since the first version, several new
90 model features have been introduced such as a comprehensive water demand and irrigation module (Wada et al.,
91 2011b, 2014), a scheme for dynamic allocation of sectoral water demand to available surface water and
92 groundwater resources and the associated calculation of return flow (de Graaf et al., 2014). These features
93 essentially introduced a two-way interaction between water demand, water withdrawal, water consumption and
94 availability, particularly over irrigated areas where water demand is large and return flow is significant.
95 Nevertheless, all of these preceding studies using PCR-GLOBWB were performed at a relatively coarse resolution
96 of 30 arc-minutes, limiting their sub-regional or local applications. Additionally, some added functionalities, such
97 as the possibility to couple the land surface component of PCR-GLOBWB to a global MODFLOW-based
98 groundwater model (Sutanudjaja et al., 2011, 2014, de Graaf et al., 2015, 2017) and an extension to simulate
99 surface water temperature (van Beek et al., 2012), were incorporated in different versions based on the original
100 PCR-GLOWB 1, leading to divergent model code development.

101
102 The objective of this paper is to summarize and present the new version of the model, PCR-GLOBWB 2, which
103 consolidates all components that have been developed since the original version of the model was first introduced
104 (van Beek et al., 2011). The new version of the model, PCR-GLOBWB 2, which is able to simulate the water
105 balance at a finer spatial resolution of 5 arc-minutes, supersedes the original PCR-GLOBWB 1, which has a
106 resolution of 30 arc-minutes only¹. The finer resolution of PCR-GLOBWB 2 allows a much better representation
107 of the effects of spatial heterogeneity in topography, soils, and vegetation on terrestrial hydrological dynamics
108 (Wood et al., 2011, Bierkens et al., 2014). Likewise, it provides a better resolution for visualization that allows
109 stakeholders and decision makers to assess model simulation output more easily and directly for the places they are
110 specifically interested in (Sheffield et al., 2010, Beven and Cloke, 2012). To assess the possible improvements, this
111 paper also presents the first evaluation results from the simulation of PCR-GLOBWB 2 at 5 arc-minute resolution
112 and compares them to a 30 arc-minute version. As discharge data are commonly used in hydrological model
113 performance evaluation, the simulated river discharge of PCR-GLOBWB 2 is compared to in situ discharge
114 observations from the Global Runoff Data Centre (GRDC, 2014).

115
116 The paper is organized as follows. Section 2 provides a global description of PCR-GLOBWB 2, including its
117 model structure and the new components and functionalities that have been added since PCR-GLOBWB 1. In
118 section 3 the global application of PCR-GLOBWB 2 is demonstrated and the results from a 58-year simulation
119 (1958-2015) are evaluated against observations of discharge, total water storage and reported withdrawal data.
120 Section 4 summarizes and concludes this paper and discusses possible future developments. Section 5 provides
121 information about availability of the model code and the underlying data.

122

¹ Note that Wada et al. (2016) made a preliminary version of the model that operates at 6 arc-minutes.

123

124 **2. PCR-GLOBWB 2 – Model description**

125

126 **2.1 General overview**

127

128 PCR-GLOBWB 2 is a state-of-the-art grid-based global hydrology and water resources model. It is a component-
129 based model implementation in Python using open source PCRaster Python routines (Karssenberget al., 2010,
130 <http://pcraster.geo.uu.nl/>). The code is distributed through Github. The computational grid covers all continents
131 except Greenland and Antarctica. Currently two versions are available: one with a spatial resolution of 5 arc-
132 minutes in latitude and longitude and one with a coarser resolution of 30 arc-minutes. Typical time steps for
133 hydrology and water use are one-day while sub-daily time stepping is used for hydrodynamic river routing. For all
134 dynamic processes involved, PCR-GLOWB 2 uses a time-explicit scheme. For each grid cell and each time step,
135 PCR-GLOBWB 2 simulates moisture storage in two vertically stacked upper soil layers (S_1+S_2 in Figure 1), as well
136 as the water exchange between the soil, the atmosphere and the underlying groundwater reservoir (S_3 in Figure 1).
137 The exchange with the atmosphere comprises of precipitation, evaporation from soils, open water, snow and soils
138 and plant transpiration, while the model also simulates snow accumulation and snowmelt. Sub-grid variability of
139 land use, soils and topography is included and influences the schemes for runoff-infiltration partitioning, interflow,
140 groundwater recharge (from S_2 to S_3) and capillary rise (from S_3 to S_2). Runoff, generated by snowmelt, surface
141 runoff, interflow and baseflow, is routed across the river network to the ocean or endorheic lakes and wetlands.
142 Routing can either be simple accumulation, simplified dynamic routing using a method of characteristics, or
143 kinematic wave routing. In case the kinematic wave routing is used, it is also possible to use a (simplified)
144 floodplain inundation scheme and to simulate the surface water temperature.

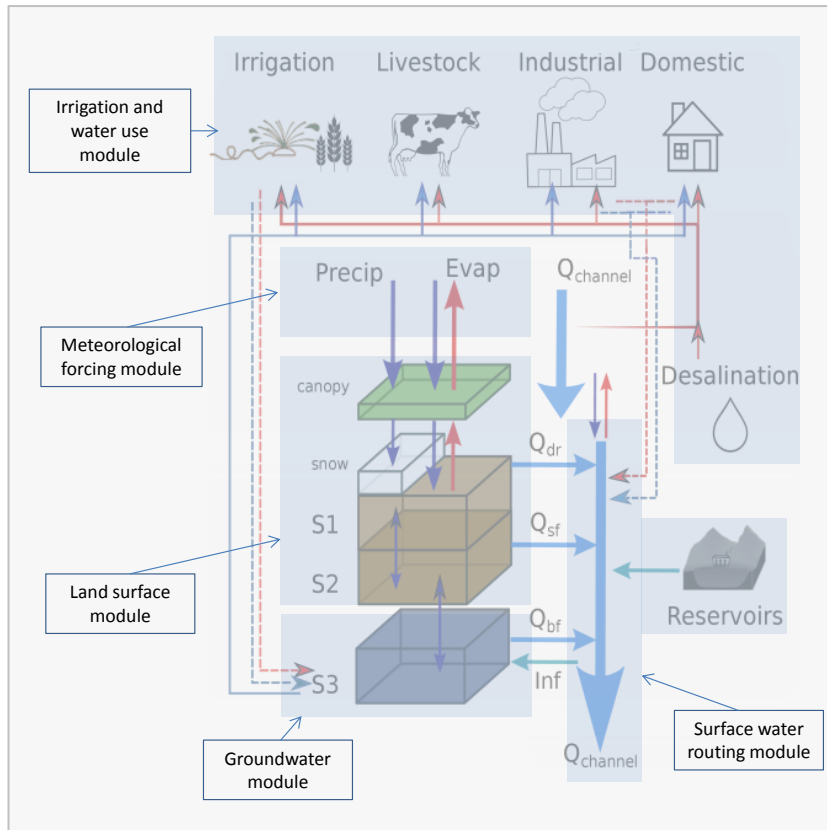
145

146 PCR-GLOBWB 2 includes a simple reservoir operation scheme that is applied to over roughly 6000 manmade
147 reservoirs from the Grand database (Lehner et al., 2011), which are progressively introduced according to their
148 construction year. Human water use is fully integrated within the hydrological model, meaning that at each time
149 step: 1) water demands are estimated for irrigation, livestock, industry and households, 2) these demands are
150 translated into actual withdrawals from groundwater, surface water (rivers, lakes and reservoirs) and desalination,
151 subject to availability of these resources and maximum groundwater pumping capacity in place, 3) consumptive
152 water use and return flows are calculated per sector.

153

154 As an option PCR-GLOBWB 2 can be partially or fully coupled to a two-layer global groundwater model based on
155 MODFLOW (de Graaf et al, 2017). Recent work (Hoch et al., 2017a,b) also includes coupling PCR-GLOBWB 2
156 to either Delft3D Flexible Mesh (Kernkamp et al., 2011) or LISFLOOD-FP (Bates et al., 2010) which are model
157 codes that can be used to solve the 1D-2D shallow water equations (or approximations thereof) for detailed
158 inundation studies.

159



161

162

163

164

165

166

167

168

169

170

Figure 1. Schematic overview of a PCR-GLOBWB 2 cell and its modelled states and fluxes. S_1 , S_2 (soil moisture storage), S_3 (groundwater storage), Q_{dr} (surface runoff – from rainfall and snowmelt), Q_{sf} (interflow or stormflow), Q_{bf} (baseflow or groundwater discharge), Inf (riverbed infiltration from to groundwater). The thin red lines indicate surface water withdrawal, the thin blue lines groundwater abstraction, the thin red dashed lines return flows from surface water use and the thin dashed blue lines return flows from groundwater use surface. For each sector: withdrawal - return flow = consumption. Water consumption adds to total evaporation. In the figure, the five modules that make up PCR-GLOBWB 2 is portrayed on the model components.

171 **2.2 Model structure and flexibility**

172

173 PCR-GLOBWB 2 has a flexible modular structure (Figure 1). The modular structure of PCR-GLOBWB 2, both in
174 terms of model concepts and implementation (separate modules are called from a main program), makes it easy to
175 modify or replace components according to specific objectives of the model application, to introduce new modules
176 or components within the modelling system and to couple it to existing codes.

177

178 There are currently five main hydrological modules in PCR-GLOBWB 2 as illustrated in Figure 1 and briefly
179 described in Section 2.3: Meteorological forcing, Land surface, Groundwater, Surface water routing, Irrigation and
180 water use. For an extensive description of the underlying equations and methods used in each of these modules we
181 refer to the following sources:

182

- 183 • Meteorological forcing module: van Beek (2008, <http://vanbeek.geo.uu.nl/suppinfo/vanbeek2008.pdf>)
- 184 • Land surface module, groundwater module and surface water routing module: van Beek and Bierkens (2009,
185 <http://vanbeek.geo.uu.nl/suppinfo/vanbeekbierkens2009.pdf>), van Beek et al. (2011,
186 <http://dx.doi.org/10.1029/2010WR009791>)
- 187 • Irrigation and water use module:
 - 188 ○ Calculation of water demand: Wada et al., (2014, <https://doi.org/10.5194/esd-5-15-2014>)
 - 189 ○ Calculation of water withdrawal, consumption and return flows: de Graaf et al. (2014,
190 <https://doi.org/10.1016/j.advwatres.2013.12.002>), Wada et al. (2014, <https://doi.org/10.5194/esd-5-15-2014>), Erkens and Sutanudjaja (2015, <https://doi.org/10.5194/piabs-372-83-2015>)

192

193 Furthermore: for details about coupling to MOFLOW we refer to:

- 194 • One-way coupling: Sutanudjaja et al. (2011, <https://doi.org/10.5194/hess-15-2913-2011>), de
195 Graaf et al. (2017, <https://doi.org/10.1016/j.advwatres.2017.01.011>)
- 196 • Two-way coupling: Sutanudjaja et al. (2014, <http://dx.doi.org/10.1002/2013WR013807>)

197

198

199 **2.3 Description of the modules**

200

201 Hereafter, we briefly describe the main features of the five modules. Additionally, a (non-exhaustive) list of the
202 model state and flux variables is provided in Table A1, whereas Table A2 lists the model inputs and parameters,
203 including their sources.

204

205 **2.3.1 Meteorological forcing module**

206

207 Meteorological forcing of PCR-GLOBWB 2 uses time series of spatial fields of precipitation, temperature and
208 reference evaporation. Reference potential evaporation can be prescribed or calculated within the model, and is
209 used in the land surface module to calculate land-cover specific potential evaporation based on crop factors of the
210 various land cover types according to the FAO guidelines (Allen et al., 1998). There are two options for calculating
211 reference potential evaporation: 1) using Hamon (1963) in case only daily mean temperature is available, 2) using
212 Penman-Monteith following the FAO guidelines (Allen et al., 1998) if net radiation, wind speed and vapour
213 pressure deficit are additionally available. See van Beek et al. (2008) for details. The resulting land-cover specific
214 potential evaporation is subsequently used to compute the actual evaporation for different land cover types in each
215 cell. Apart from the calculation of evaporation, temperature is also used to partition precipitation into snow and
216 rain and to drive snowmelt.

217

218

219 **2.3.2. Land surface module**

220

221 This core module of PCR-GLOBWB 2 covers the land-atmosphere exchange, the vertical flow between soil
222 compartments and the eventual groundwater recharge, snow and interception storage and the runoff generation
223 mechanisms. These processes are simulated over a number of land cover types and aggregated proportionally
224 based on land cover fractions within a model cell. Users can specify their own land cover classification and
225 introduce their own land cover parameterization. The number of land cover types is configurable. The standard
226 parameterization of PCR-GLOBWB 2 carries four land cover types consisting of tall natural vegetation, short
227 natural vegetation, non-paddy irrigated crops, and paddy irrigated crops (i.e. wet rice). There is also a
228 parameterization set for six land cover types (Bosmans et al., 2017), albeit still at 30 arc minute resolution only,
229 that includes distinct types for pasture and rain-fed crops. For the standard four land cover parameterization of
230 PCR-GLOBWB, applied in this paper, the land cover types of pasture and rain-fed crops are integrated into the
231 short natural vegetation type.

232

233 For each land cover type, separate soil conditions can be specified. It should be noted that the soil and vegetation
234 conditions are in any case fully spatially distributed. Thus, vegetation properties (e.g., crop factor, Leaf Area
235 Index) and soil properties (depth, saturated hydraulic conductivity, etc.) vary not only between land cover types,
236 but may also vary from cell-to-cell (e.g., per climate zone). In the standard parameterization vegetation properties
237 vary over the year using a monthly climatology of phenology and crop calendars (i.e. for the crop factor and LAI).
238 The application of irrigation water for paddy and non-paddy irrigation is done by the irrigation and water use
239 module. It is based on the FAO guidelines of Allen et al. (1998) and is dependent on the actual soil water storage
240 (S_1 , S_2) or paddy-open water storages. All fluxes, from and to the land surface module in Figure 1, are thus
241 calculated separately per land cover type. The resulting vertical fluxes for each land cover type are: interception

242 evaporation, bare soil evaporation, snow sublimation, vegetation-specific transpiration. In the soil column, vertical
243 fluxes are driven by degrees of saturation of soil layers and interact with the underlying groundwater store, S_3 (see
244 e.g. van Beek and Bierkens, 2009; Sutanudjaja et al., 2011; Sutanudjaja 2012 for detailed explanation). Surface
245 runoff (Q_{dr} , from precipitation and snowmelt) consists of infiltration excess runoff and saturation excess runoff
246 following a sub-grid approach that mimics variable source areas, i.e. the improved Arno Scheme (Todini, 1996,
247 Hagemann and Gates, 2003). Interflow or stormflow (Q_{sf}), mostly occurring in regolith soils on hillslopes, is also
248 handled with a sub-grid approach based on a runoff parameterization by Sloan and Moore (1984). All fluxes are
249 computed per land cover type and balanced with the available storage to arrive at the net flux that is used to update
250 the storages for the next time step. Also, to report the overall fluxes per cell, and to pass these to other modules, the
251 land cover specific fluxes are subsequently averaged (weighted by land cover type fractions).

252

253 For the standard parameterization of the land surface module the following data sets are combined (see Table A2):
254 the cell fractions of various non-irrigation land cover types are based on the map of Global Land Cover
255 Characteristics Data (GLCC) Base Version 2.0 (Loveland et al., 2000) with the land cover classification following
256 Olson (1994a, b) and the parameter sets from Hagemann et al. (1999) and Hagemann (2002). Irrigation land cover
257 types (i.e. paddy and non-paddy), including their crop calendars and growing season lengths, are parameterized
258 based on the data set of MIRCA2000 (Portmann et al., 2010) and the Global Crop Water Model of Siebert and Döll
259 (2010). We refer to van Beek et al. (2011) for detailed descriptions.

260

261 **2.3.3. Groundwater module**

262

263 The groundwater module calculates groundwater storage dynamics subject to recharge and capillary rise
264 (calculated by the land surface module), groundwater discharge (Q_{bf} , in case of a positive groundwater storage) and
265 riverbed infiltration (Inf). Groundwater discharge (assumed the same as groundwater baseflow here) depends on a
266 linear storage-outflow relationship ($Q_{bf} = S_3/J$) where the proportionality constant J is calculated following
267 drainage theory of Kraijenhoff-van de Leur (1958) based on drainage network density and aquifer properties.
268 Riverbed infiltration occurs only in case Q_{bf} becomes 0 by groundwater withdrawal. Under persistent groundwater
269 withdrawal (calculated with the Irrigation and Water use module) that is larger than the sum of recharge and
270 riverbed infiltration, the groundwater storage S_3 is allowed to become negative. In this case, the part of the
271 withdrawn groundwater in excess of the input (recharge and riverbed infiltration) is seen as non-renewable
272 groundwater withdrawal leading to groundwater depletion (permanent loss of groundwater from storage). In case
273 withdrawal becomes smaller than the input, the remaining input is used to first fill the negative storage to zero,
274 before baseflow Q_{bf} commences again. As an alternative, it is also possible to limit the maximum volume of non-
275 renewable groundwater that can be extracted. .

276

277 It is possible to use a full-fledged groundwater flow model based on MODFLOW (Harbaugh et al., 2000) coupled
278 to PCR-GLOBWB 2 in order to calculate groundwater heads and flow paths. This can be done as a one-way

279 coupling where PCR-GLOWB 2 is first run with the standard groundwater module (reservoir S_3 with only vertical
280 fluxes) to yield time series of net groundwater recharge (recharge – capillary rise) and surface water levels. These
281 fluxes/inputs are subsequently used to force the groundwater flow model (see e.g.
282 Sutanudjaja et al., 2011, de Graaf et al., 2017). Another possibility is to use a two-way coupling where the
283 groundwater module of PCR-GLOBWB 2 is replaced by the groundwater flow model. In this case, at each time
284 step fluxes are exchanged between the groundwater model and the land surface module, and the groundwater
285 model and the surface water routing module (Sutanudjaja et al. 2014).

286
287

288 **2.3.4 Surface water routing module**

289

290 Following an 8-point steepest gradient algorithm across the terrain surface (local drainage direction or LDD), all
291 cells of the modelled domain are connected to a strictly convergent drainage network that together makes up the
292 river basins and sub-basins of the model domain. The lowermost cell is either connected to the ocean or to an
293 endorheic basin. Per cell, the sum of the three daily runoff fluxes (Figure 1) is aggregated and routed along the
294 drainage network until passing the lowermost cell and being removed from the model. Routing can be done in
295 three ways of increasing complexity: 1) simple accumulation of the fluxes over the drainage network; 2) a travel-
296 time characteristic solution (Karssenberget al., 2007), and 3) the kinematic wave solution.

297

298 The first method is typically aggregated over longer time steps (e.g. month or year) that are larger than the travel
299 times of water along the longest river length. The second routing method includes an estimation of cell flow
300 velocity based on average discharge from the last 5 years and Manning's equation, which assumes the energy slope
301 to be equal to the bed slope. This estimated velocity is used to move the volume of water in the channel of a cell
302 the corresponding distance within one daily time step along the drainage network. This method works reasonably
303 well for relatively steep rivers in humid climates where the friction slope is close to the bed slope and the rivers are
304 equally filled with water throughout the year. The third method is the kinematic wave approximation of the Saint
305 Venant equations with flow described by Manning's equation. Also, here, it is assumed that friction slope and bed
306 slope are equal, which makes it valid for rivers without backwater effects. The kinematic wave is solved using a
307 time-explicit variable sub-time stepping scheme based on the minimum Courant number. Of these methods, the
308 kinematic wave solution simulates the propagation of the flood wave more realistically while the others provide an
309 expedient means to approximate discharge over longer periods.

310

311 Using the kinematic wave method, it is possible to model floodplain inundation which occurs if the discharge
312 exceeds the bankfull capacity of a channel. The excess discharge volume is spread over the entire cell from the
313 lowest part of the cell (based on a higher resolution sub-grid DEM) yielding a flooded area with an approximated
314 flood depth. In case of flooding, the simulated river flow is impacted by adjusting the wetted area and wetted

315 perimeter and calculating a weighted Manning coefficient from the individual Manning coefficients of the
316 floodplains and the channel.

317

318 Lakes and reservoirs are part of the drainage network. Lakes and reservoirs can extend over multiple cells, in
319 which case the storage is subdivided by area such as to ensure that lake and reservoir levels are the same across
320 their extent. The active storage of lakes and the actual storage of reservoirs are dynamically updated, for the lake
321 outflow a standard storage-outflow relationship based on a rectangular cross-section over a broad-crested weir
322 (Bos, 1989) is used, while reservoirs follow a release strategy. This strategy is, by default, aimed at passing the
323 average discharge, while maintaining levels between a minimum and maximum storage (Wada et al., 2014), but
324 more elaborate strategies that take account of downstream water demand are possible (e.g. van Beek et al., 2011).
325 Lakes and reservoir areas change based on global volume-area relationships. All surface water areas, which can be
326 classified into several water types, river channels, inundated floodplains, lakes and reservoirs, are subject to open
327 water evaporation calculated from reference potential evaporation multiplied with factors depending on water types
328 and depths. Moreover, surface waters are subject to surface water withdrawal calculated with the Irrigation and
329 Water Use module.

330

331 If the kinematic wave approach is used, it can be also augmented with an energy routing scheme to simulate
332 surface water temperature (van Beek et al., 2012). Finally, it should be noted that it is possible to run the routing
333 routine from PCR-GLOBWB 2 as a stand-alone routine, which allows it to be fed with the specific discharge from
334 other land surface models.

335

336 The routing methods that are available in PCR-GLOBWB 2 will yield significant errors for wide lowland rivers
337 where backwater effects are important. In this case, it is possible to replace the surface water module for part of the
338 modelling domain with hydrodynamic models solving the shallow water equations (Hoch et al., 2017a). Hoch et al.
339 (2017b) developed a generic coupler for this purpose that enables coupling to multiple hydrodynamic modelling
340 codes (<https://doi.org/10.5281/zenodo.597107>).

341

342 Although any data set can be used to define the drainage network and locate the lakes and reservoirs, the standard
343 parameterization of PCR-GLOBWB 2 that runs globally uses the drainage network derived from the high
344 resolution 30 arc-sec HydroSHEDS (Lehner et al., 2008) combined with 30 arc-sec GTOPO30 (Gesch et al., 1999)
345 and 1 km Hydro1k (Verdin and Greenlee, 1996, USGS EROS Data Center, 2006), lakes taken from GLWD
346 (Lehner and Döll, 2004) and reservoirs obtained from Grand (Lehner et al., 2011).

347

348 **2.3.5 Irrigation and water use module**

349

350 In PCR-GLOWB 1 water demand was calculated separately from the hydrology and water availability calculated
351 as a post-processing step by subtracting upstream demand (Wada et al., 2011a,b). In PCR-GLOBWB 2 water use
352 (withdrawal and consumption) is fully integrated. Hereafter, the main features of the irrigation and water use
353 module are described in the following order: water demand, water withdrawal, water consumption and return
354 flows.

355

356 Water demand

357

358 *Irrigation water demand* is calculated based on the crop composition (which changes per month and includes
359 multi-cropping) and the irrigated area per cell. As stated above, these are obtained from MIRCA2000 (Portmann et
360 al., 2010) and the Global Crop Water Model (Siebert and Döll, 2010). In the standard PCR-GLOBWB 2
361 parameterization the irrigated areas change over time. In want of detailed data, fractions of paddy and non-paddy
362 irrigation, as well as the crop composition per month stay fixed (as obtained from MIRCA2000), while the total
363 irrigated area per cell changes over time and is based on the FAOSTAT (FAO, 2012) reported irrigated areas.

364 Irrigation water demand is computed using the FAO guidelines (Doorenbos and Pruit, 1977, Allen et al., 1998): in
365 case of non-paddy irrigation, water is applied whenever soil moisture falls below a pre-set value and then the soil
366 column is replenished up to field capacity. In case of paddy irrigation, the water level is kept at a water depth of 5
367 cm above the surface until the late crop development stage (~ 20 days) before the harvest. After that, no irrigation
368 is applied anymore such that the water level is allowed to drop to zero under infiltration and evaporation (Wada et
369 al., 2014). The net irrigation demand is augmented to account for limited irrigation efficiency and losses. In order
370 to obtain irrigation water demand including losses, i.e. gross irrigation demand, net irrigation water demand is
371 multiplied with $(1 + f_i)$, with f_i a country-specific loss factor obtained from Rohwer et al. (2007).

372

373 *Non-irrigation water demand* covers three sectors, industry, households and livestock. For each of these sectors,
374 the gross demand and net demand are prescribed to the model. The calculation of net non-irrigation water demand,
375 which varies with time, follows methods developed by Wada et al (2014). We refer to Wada et al. (2014) for an
376 extensive description. Trends in water demand are prescribed on an annual basis as a function of population,
377 electricity demand and gross domestic product (GDP) per capita. In addition, domestic water demand exhibits a
378 seasonal variation on the basis of temperature. Domestic and industrial gross water demand is calculated from net
379 water demand using a country-specific recycling ratio RC (based on development stage or GDP per capita and
380 additionally access to domestic water demand): $gross = net/(1-RC)$. This takes into account that much of the
381 domestic and industrial water is not consumed but returned as surface water. For livestock, the return flow is
382 assumed to be zero, meaning all water is consumed.

383

384

385 Water withdrawal

386

387 The water withdrawal estimation is based on the work by de Graaf et al. (2014) and Wada et al. (2014). In PCR-
388 GLOBWB 2 water withdrawal is set equal to gross water demand (summed over all the sectors) unless sufficient
389 water is not available. In that case, water withdrawal is scaled down to the available water and then allocated
390 proportionally to gross water demand per sector. Thus, no allocation preference is available in the standard
391 parameterization of PCR-GLOBWB 2.

392

393 Water can be abstracted from three sources: surface water, groundwater (fossil and non-fossil) and desalinated
394 water. The latter is prescribed (Wada et al., 2011a), while the fractions of the other two sources are determined as a
395 function of their relative abundance. Groundwater and surface water availability are determined based on two-year
396 running means of groundwater recharge and river discharge respectively, thus keeping track of the prevalence of
397 local resources and their temporal change (de Graaf et al., 2014). These fractions determine on a monthly basis
398 from which source water is abstracted. Surface water withdrawal is ceased if river discharge falls below 10% of the
399 long-term average yearly discharge under naturalized flow conditions (determined by running the model without
400 withdrawal). If, for some reason, the surface water amount is insufficient, the model falls back on groundwater to
401 meet the resulting gap. Groundwater is first abstracted from the renewable groundwater storage, and if this is not
402 present, non-renewable groundwater is abstracted. The amount of groundwater that can be abstracted is, however,
403 capped by the groundwater pumping capacity which is based on data by IGRAC GGIS database. The described
404 dynamic allocation scheme is not always in line with local preferences or the infrastructure. However, there is a
405 possibility to use fractions of groundwater and surface water withdrawal reported in the literature. For urban areas,
406 we rely on the data set of McDonald et al. (2014) that states whether a surface water distribution infrastructure is
407 available. If this is the case, industrial and domestic water withdrawals are mainly taken from surface water before
408 abstracting groundwater. If surface water infrastructure is limited, groundwater source is prioritized (see e.g.
409 Erkens and Sutanudjaja, 2015). For urban areas that are not in the McDonald (2014) data set, we give preference to
410 the dynamic allocation scheme. For irrigation, we use the ratios supplied by Siebert et al. (2010) in regions where
411 they are said to be reliable. In regions where they are not fully reliable, we take the average ratio provided by
412 Siebert et al. (2010) and the one provided by the dynamic allocation scheme. For regions where the data of Siebert
413 (2010) are not reliable (i.e., extrapolated data), we give preference to the dynamic allocation scheme.

414

415 Moreover, we cannot assume that all the water demand is supplied from surface water and groundwater resources
416 in the same cell. Ideally, data about local water redistribution networks and inter-basin transfers should be used to
417 define surface water and groundwater service areas. Unfortunately, this information is not available at the global
418 scale. Therefore, in our current parameterization of PCR-GLOBWB 2, we pool water availability of desalinated
419 and surface water over zones of approximately 1 arc-degree by 1 arc-degree size that are truncated by country

420 borders if applicable. For groundwater, 0.5 arc-degree zones are used. The downside of the current scheme is that a
421 cell does not always have access to its nearest water resource if this lies outside its prescribed service area.

422

423 Water consumption and return flows

424

425 In case of irrigation, all the withdrawn water is applied to the soil (non-paddy) or the water level on the field
426 (paddy). Part of that water is lost by transpiration and part by soil and open water evaporation. Transpiration and
427 evaporation together make up the irrigation water consumption. The remaining part of irrigated water is lost by
428 percolation and contributes to groundwater recharge as return flow. Irrigation efficiency (not including conveyance
429 losses) could also be calculated after the fact by the difference between withdrawal and transpiration. In case of
430 domestic and industrial water use, water consumption depends on the recycling ratio RC and equals
431 $\text{withdrawal} \times (1 - \text{RC})$, while $\text{withdrawal} \times \text{RC}$ constitutes return flow. All return flow is added to the surface water.
432 For livestock, the consumption is set equal to the withdrawal and no return flow is assumed.

433

434 **2.4 Model code**

435

436 The original PCR-GLOBWB version 1 (van Beek et al., 2011) was written in the PCRaster scripting language.
437 PCRaster (Wesseling et al., 1996) is a high-level programming language that started as a dynamic raster-based
438 Geographical Information System (GIS) and is tailored to spatiotemporal modelling for environmental and earth
439 science applications. The generic nature of PCRaster with its many pre-existing built-in hydrological functions and
440 its syntax that reads like pseudo-code, generally results in concise model codes, short development times and
441 limited programming errors. Karssenberget al. (2010) developed a PCRaster Python package such that PCRaster
442 functions, implemented in C++, can also be called via Python (<http://www.python.org/>). Using PCRaster Python
443 makes it possible for students and beginner modellers to contribute to the model quickly, while it allows experts to
444 be more productive and focus on the science rather than on the programming language syntax. Realising the
445 aforementioned advantages, PCR-GLOBWB, particularly starting from this version 2, has been rewritten in the
446 Python scripting language.

447

448 To allow for exchanges of model components and, therefore, evaluate different model configurations, a
449 component-based development approach (e.g Argent, 2004; Castronova and Goodall, 2010) was followed while
450 developing the PCR-GLOBWB 2 model code. Each of the PCR-GLOBWB scientific modules described in section
451 2.3 is implemented in a separate Python class that needs to implement initialization and update methods. The latter
452 designates changes of states and fluxes per time step. Each of module is initialized and executed by iteratively
453 calling the update method via a main model script.

454

455 To run the model a so-called initialization file or configuration file is used (with extension .ini). In this file the
456 following aspects are defined: the spatial and temporal domain, the time step, the settings of the different modules
457 (e.g. which surface water routing, human water use or not etc.) and the locations and names of the parameter files
458 and forcing files. PCR-GLOBWB 2 uses NetCDF files for most input and all output, thus making it easier to
459 exchange data with other scientists and use existing tools to analyse its output.

460

461 PCR-GLOBWB 2 generally runs best under Linux. In order to run PCR-GLOBWB the following additional
462 software needs to be installed: PCRaster version 4, Python versions 2.7 with Python packages numPy and netCDF4
463 and gdal version 1.8 or higher.

464

465 **2.5 Differences between PCR-GLOBWB 1 and 2**

466

467 PCR-GLOBWB 2 has the following new capabilities compared to PCR-GLOBWB 1 (cf. van Beek et al., 2011,
468 Wada et al, 2011):

- 469 • the model was completely rewritten in PCRaster Python and now has a modular structure,
- 470 • the inputs and outputs are in the form of NetCDF files and output can be reported for daily monthly and yearly
471 time steps,
- 472 • parameterizations are available at 30 arc-minute and 5 arc-minute resolutions,
- 473 • water use (demand, withdrawal, consumption and return flow) is fully integrated,
- 474 • distinction is made between paddy and non-paddy irrigation and irrigation follows FAO guidelines,
- 475 • three different options for surface water routing are available and a surface water temperature module is fully
476 integrated with the routing scheme,
- 477 • it is possible to run surface water routines separately with specific discharge from other sources (e.g. other
478 land surface models),
- 479 • PCR-GLOBWB 2 can be coupled to a two-layer transient groundwater model (Sutanudjaja et al., 2014, de
480 Graaf et al., 2017) and to the hydrodynamic models Delft3D Flexible Mesh (Kernkamp et al., 2011) or
481 LISFLOOD-FP (Bates et al., 2010, see Hoch et al., 2017b).

482

483

484 **3. Model demonstration and evaluation**

485

486 To test and evaluate the performance of PCR-GLOBWB 2, we ran the model at both 30 arc-minute and 5 arc-
487 minute resolution over the period 1958-2015. We compared the results of both simulations with discharge data
488 from the Global Runoff Data Centre (GRDC, 2014), with total basin water storage estimates from GRACE
489 (Gravity Recovery and Climate Experiment, Wiese, 2015) and with water withdrawal data from the FAO
490 AQUASTAT database (FAO, 2016).

491

492

493 **3.1 Model run setup**

494

495 **3.1.1 Parameterization**

496

497 We used the standard parameterization (parameters, forcing and their sources in Table A2) of PCR-
498 GLOBWB 2 at 30 arc-minute and 5 arc-minute spatial resolutions to simulate global hydrology at daily
499 resolution over 1958-2015. Outputs were reported as monthly averages. The parameterization was mostly
500 unchanged from that given in van Beek and Bierkens (2009), but newer datasets were used if available,
501 such as the GRAND (Lehner et al., 2011) dataset for reservoirs and MIRCA (Portmann et al., 2010) for

502 crop areas. We stress that no calibration was performed. We ran the model with human water use options
503 turned on and used the travel-time characteristic solution routing option.

504

505 **3.1.2 Forcing**

506

507 The forcing data set is based on time series of monthly precipitation, temperature and reference evaporation
508 from the CRU TS 3.2 data set of Harris et al. (2014) downscaled to daily values with ERA40 (1958-1978,
509 Uppala et al., 2005) and ERA-Interim (1979-2015, Dee et al., 2011). CRU is specified at 30 arc-minute
510 spatial resolution and directly usable. We used ERA40 and ERA-I results that had been resampled by
511 ECMWFs resampling scheme from their original resolutions ($\sim 1.2^\circ$ and $\sim 0.7^\circ$) to 30 arc-minutes first. Here,
512 resampling means a form of spatial downscaling whereby the values of the larger ERA40 and ERA-I grid
513 cells are assigned to the cell centers and then spatially interpolated onto 30 arc-minute grids. Precipitation
514 was temporally downscaled by first applying a threshold of 0.1 mm/day to the ERA daily time series to
515 estimate the number of rain days for ERA. The amount of rainfall below this threshold was proportionally
516 allocated to the rain days. Next, the daily rainfall totals were scaled in order to reproduce the CRU monthly
517 precipitation total using multiplicative scaling. Equally, monthly reference potential evaporation, computed
518 with Penman-Monteith from the CRU data set, was scaled using multiplicative scaling and downscaled to
519 daily data proportional to Hamon (1967) evaporation calculated from daily ERA temperatures. We elected
520 not to calculate Penman-Monteith reference evaporation directly from the ERA40 and ERA-I data, in order
521 to avoid the large calculation times needed to process the required meteorological values. For the air
522 temperature, an additive scaling factor was used. To better simulate snow-dynamics for the 5arc-minute
523 model, the temperature values from CRU were further spatially downscaled to 5 arc-minutes using a
524 temperature lapse-rate derived from the higher-resolution CRU CL 2.0 climatology (New et al., 2002). For
525 areas where the number of stations underlying the CRU data set was found to be small, preference was
526 given to using directly the meteorological data from ERA. The method used to create the forcing data set is
527 described more extensively in van Beek (2008).

528

529 **3.1.3 Spin-up**

530

531 The large groundwater response times for certain regions (e.g. Niger and Amazon) requires substantial
532 spin-up for the groundwater volumes to be in equilibrium with the current climate. To reach this
533 equilibrium, the model was spun-up using the average climatological forcing over the years 1958–2000
534 back-to-back for 150 years to reach a dynamic steady state. This spin-up was executed under naturalized
535 condition which means no reservoirs and no human water use.

536

537 **3.1.4 Computation time and parallelization**

538

539 The models were run on Cartesius, the Dutch national supercomputer
540 (<https://userinfo.surfsara.nl/systems/cartesius>). Without parallelization, the wall clock time for a one-year
541 global simulation run of the 30 arc-minute model was about one hour. This entails that a one-year global
542 simulation run with the 5 arc-minute model, might result in wall clock times of at least 36 hours. Hence, to
543 speed-up computation, the 5 arc-minute model domain was divided into 53 groups of river basins such that
544 it could be run as 53 separate processes. With this simple parallelization technique, the wall clock time for a
545 one-year simulation run of the 5 arc-minute model reduced to about one hour again. Note that these
546 computation times were obtained for simulations with the travel-time characteristic routing option. Calculation
547 times would have been significantly longer if the kinematic wave routing had been used (e.g. about 6 hours for a
548 one-year 5 arc-minutes global run including parallelization).

549

550 **3.2 Data used for comparison**

551

552 **3.2.1 River discharge**

553

554 We used discharge stations from GRDC (2014) to compare simulated discharge from PCR-GLOBWB 2
555 with monthly reported discharge. From all the globally available stations in the database, we selected a
556 subset of stations using the following criteria: 1) allowing a not more than 15% difference in catchment
557 area between PCR-GLOBWB 2 and the area reported with the GRDC discharge station, 2) not more than 1
558 cell distance between the station location and the nearby location of a river in PCR-GLOBWB 2, 3) at least
559 1 year of discharge data. This yielded 5363 stations for the 5 arc-minute simulation, 3910 stations for the 30
560 arc-minute simulation and 3597 stations fulfilling the criteria for both resolutions. The minimum, median
561 and maximum catchment sizes for the GRDC stations at the 5 arc-minute resolution are respectively 29,
562 2730 and $4.68 \cdot 10^6 \text{km}^2$ and 31, 6560 and $4.68 \cdot 10^6 \text{km}^2$ at the 30 arc-minute resolution. As we jointly
563 compared the performance of both simulations, we used the set of 3597 locations throughout. The average
564 time series length of these stations is equal to 36 years.

565

566 **3.2.2 Total water storage**

567

568 We compared total water storage (TWS) as simulated by PCR-GLOBWB 2 with the TWS estimated from
569 GRACE (Gravity Recovery and Climate Experiment) gravity anomalies. We used the GRACE JPL Mascon
570 product PL-RL05M (Wiese, 2015, Watkins et al., 2015, Wiese et al., 2016). Scanlon et al. (2016) suggest
571 that recent developments in mascon (mass concentration) solutions for GRACE have significantly
572 increased the spatial localization and amplitude of recovered terrestrial TWS signals. They also claim that
573 one of the advantages of using the mascon solutions relative to traditional SH (spherical harmonic)

574 solutions is that it makes it much easier for non-geodesists to apply GRACE data to hydrologic problems.
575 Note that although the data of PL-RL05M are represented on a 30 arc-minutes lat-lon grid, they represent
576 the 3x3 arc-degree equal-area zones, which is the actual resolution of JPL-RL05M. We compared trends on
577 a pixel-by-pixel basis. Given the coarse resolution of GRACE products of about 300 km by 300 km we
578 compared correlations only for major river basins with an area of 900,000 km² and up.

579
580

581 **3.2.3 Water withdrawal**

582

583 The water withdrawal for a large number of countries is taken from FAO's AQUASTAT database (FAO,
584 2016). This data is on average reported in every 5 years. We compared simulated water withdrawal per
585 sector and per water source (surface water and groundwater) with reported values per country and per
586 reporting period, whenever available.

587

588

589 **3.3 The global water balance simulated at 30 and 5 arc-minutes**

590

591 We calculated the main global water balance components from the 30 arc-minute and 5 arc-minute
592 simulations over the period 2000-2015. The results in Table 1 show that there are some differences between
593 the two model runs, but values are in the same order of magnitude. The small difference in precipitation is
594 due to the fact that the area of the land cells is slightly different at the two resolutions. Differences in
595 evaporation and runoff show that the runoff and evaporation parameterization of PCR-GLOBWB 2 is not
596 entirely scale-consistent. Differences in evaporation may also be causing the differences in irrigation water
597 demand which in turn may explain the differences in water withdrawal. Recently, Samaniego et al. (2017)
598 applied their multiscale parameter regionalization (creating spatially variable parameter fields) technique
599 (MPR) to PCR-GLOBWB 2 for the Rhine basin, showing that parameterizations that yield the same
600 hydrological fluxes at different resolutions are possible. However, a global application of this method to all
601 PCR-GLOWB 2 parameters is not possible yet. Nonetheless, when comparing the results of both model
602 runs with data reported in the literature, it shows that the global water balance components are similar to
603 recent assessments (e.g. by Rodell et al., 2015) and groundwater withdrawal and total withdrawal estimates
604 match those of previous studies (see Table 2).

605

606 From Table 1, it can also be seen that there is a negative change in total terrestrial water storage in both
607 model runs. Table 1 shows that this can only be partly explained by groundwater depletion, which is
608 localized to certain regions (see also Sect. 3.4.2). Further analysis shows that this change can also be
609 attributed to the trends in precipitation forcing used, particularly over the tropics.

610 *Table 1. Global Water balance components and human water withdrawal (in km³/year and mm/year) over*
611 *the period 2000-2015 as obtained from the 30 arc-minutes and the 5 arc-minute simulations. The numbers*
612 *are shown to high significance to show the water balance closure. This does not mean that we pretend to*
613 *know e.g. global discharge with a km³ accuracy (actual accuracy of the large fluxes is more in the order of*
614 *10³ km³)*

		30 arc-min		5 arc-min	
		km ³ /year	mm/year	km ³ /year	mm/year
Global water balance	Precipitation	107452	808	107495	811
	Desalinated water use	3	0.02	2	0.01
	Runoff	42393	319	43978	332
	Evaporation*	65754	494	63974	483
	Change in total water storage	-693	-5	-455	-3
Groundwater budget	Groundwater recharge	27756	209	25521	193
	Groundwater withdrawal	737	6	632	5
	Non-renewable groundwater withdrawal (groundwater depletion)	173	1	171	1
	Renewable groundwater withdrawal	564	4	460	3
Withdrawal by sector	Agricultural water withdrawal (irrigation + livestock)	2735	21	2309	17
	Domestic water withdrawal	380	3	314	2
	Industrial water withdrawal	798	6	707	5
Withdrawal by source	Total water withdrawal	3912	29	3330	25
	Surface water withdrawal	3172	24	2697	20
	Desalinated water use	3	0.02	2	0.01
	Groundwater withdrawal	737	6	632	5

615 * Includes consumptive water use for livestock, domestic and industrial sectors

616

617

618 *Table 2. Groundwater withdrawal and total water withdrawal as compared to other studies (in km³/year)*

Source		Year	Value (km ³ /year)
Groundwater withdrawal	Wada et al. (2010) (from the IGRAC database)	2000	734 (±87)
	Döll et al. (2012)	1998-2002	571
	Döll et al. (2014) (their Table 2).	2003-2009	690-888
	Döll et al. (2014) (their Table 6).	2000-2009	665
	Pokhrel et al. (2015)	1998-2002	570 (±61)
	Hanasaki et al. (2018)	2000	789 (±30)
	This study (5 arc-minutes)	2000-2015	632
Total water withdrawal	Vörösmarty et al. (2005)	1995-2000	3560
	Oki and Kanae (2006)	contemporary	3800
	Döll et al. (2012)	1998-2002	4340
	Döll et al. (2014) (their Table 2)	2003-2009	3000-3700
	FAO (2016)	2010	3583
	Hanasaki et al. (2018)	2000	3628 (±75)
This study (5 arc-minutes)	2000-2015	3330	

619

620

621 **3.4 Evaluation of the 30 and 5 arc-minute simulations**

622

623 **3.4.1 Discharge**

624

625 When evaluating the simulated discharge with discharge observations from GRDC, we used the monthly
626 values and calculated three different measures. The first one is the correlation coefficient between monthly
627 simulated and observed GRDC time series, which is a measure of reproducing correct timing of high and
628 low discharge. A correlation coefficient of 1 indicates perfect timing. The second measure is the Kling-
629 Gupta efficiency coefficient or KGE (Gupta et al., 2009) which equally measures bias, differences in
630 amplitude and differences in timing between monthly simulated and observed GRDC time series. The KGE
631 varies between 1 and minus infinity, where 1 means a perfect fit in terms of bias, amplitude and timing. The
632 last metric is the anomaly correlation, i.e. the correlation between monthly time series after the seasonal
633 signal (climatology) has been removed. This statistic measures the ability of the model to correctly simulate
634 timing of seasonal and the inter-annual anomalies from the yearly climatology. This is to test if the model is
635 able to capture the monthly scale and inter-annual anomalies in discharge (i.e. on the monthly scale) when
636 the dominant seasonal trend is removed from observations and simulations. An anomaly correlation of 1
637 indicates perfect characterization of inter-annual anomalies and values below 0 indicate a lack thereof.

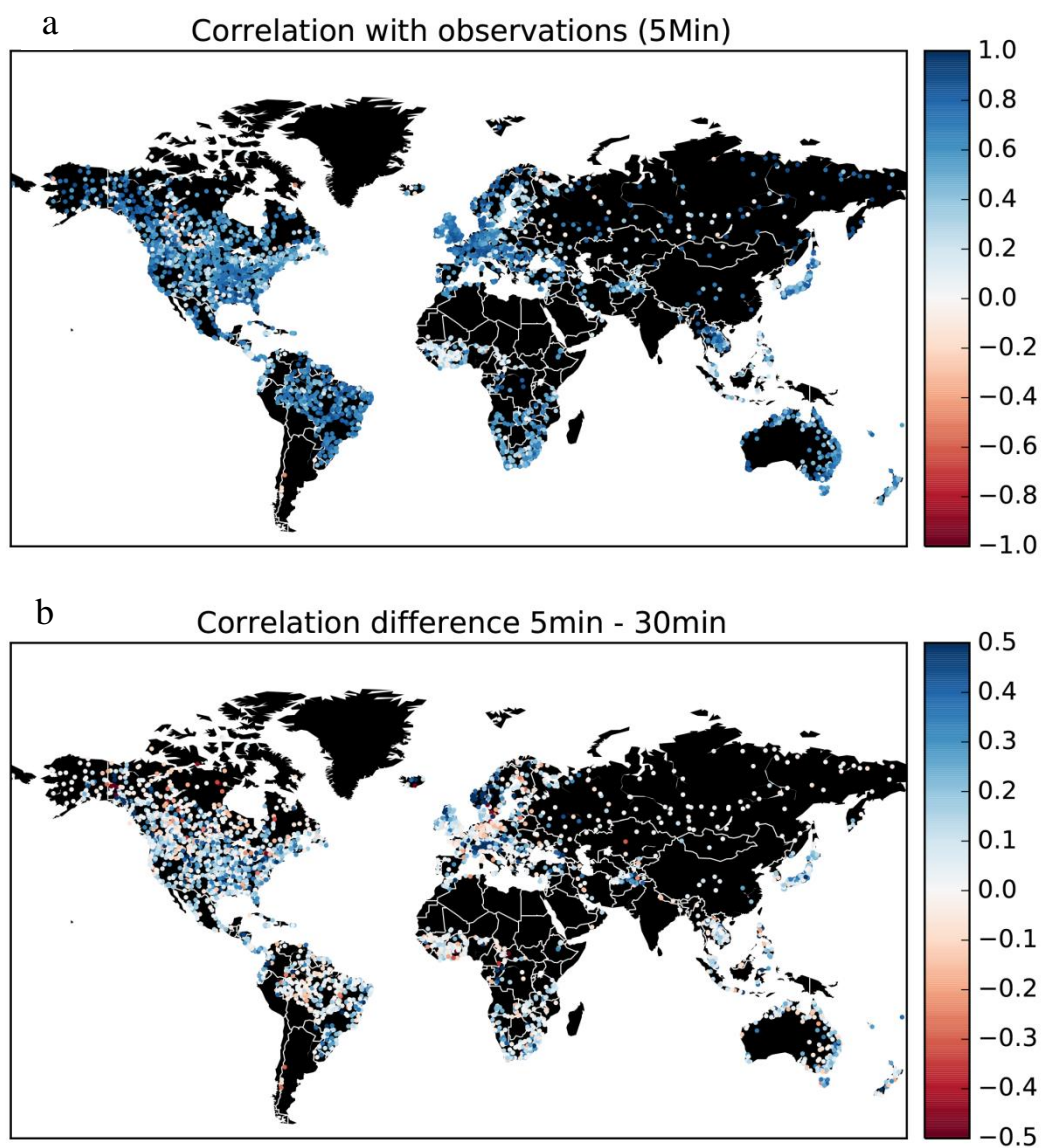
638

639 Figure 2 shows maps of the correlation coefficients for the GRDC stations considered and Figure 3 shows
640 histograms of correlation and KGE values. Both figures show that the evaluation results of the 5 arc-minute
641 simulation are generally better than those of the 30 arc-minute simulation. For the 30 arc-minute model, the
642 number of catchments with KGE > 0, 0.3 and 0.6 are equal to 48%, 26% and 7% of the total catchments
643 respectively. For the 5 arc-minute model, these values are respectively equal to 63%, 40% and 12% of the
644 total catchments. Note that for both runs the standard parameterization was used. Possible explanations for
645 the better performance of the 5 arc-minute run are: a better delineation of the shape of the basins,
646 particularly the smaller ones, a better characterization of basin relief and the drainage network, more
647 accurate sub-grid parameterization of soil and land cover due to a smaller scale-gap that needs to be
648 overcome, better estimates of the basin storage and better snow dynamics due to the downscaling of
649 temperature to 5 arc-minute resolution. The KGE values are less favourable than the correlation
650 coefficients. This is mostly due to biases in runoff caused by incorrect meteorological forcing. It is difficult
651 to exactly assess which of these factors are most important in determining the improvement. Inspecting the
652 histograms of correlation and KGE (Figure 3) shows that the improvement is mostly apparent for the
653 smaller sized catchments, which supports the notion that a better delineation of the catchments' shape,
654 topography and drainage network could be the cause. However, disentangling these individual effects
655 would require further study. To investigate the possible effects of better snow dynamics we classified the
656 GRDC stations into stations below 1000 m altitude (above mean sea-level) and those above 1000 m. The
657 GRDC stations above 1000 m are expected to experience precipitation falling as snow during periods of the

658 year. The results in Figure 4 clearly show that the improvement is larger for the higher GRDC stations, This
659 supports the explanation that better snow dynamics due to temperature lapsing in combination with a better
660 resolved digital elevation model is partly responsible for the superior results at 5 arc-minutes. We also
661 investigated if improvements were notably different between climate zones, by separately calculating
662 KGEs for GRDC stations in the Köppen-Geiger zones A (Tropical), B (Desert), C (Temperate) and D
663 (Continental). The results (not shown) show that the improvement is equally visible for climate zones A, B
664 and C and less so for D (continental). Without further analysis this is difficult to explain. Note however that
665 the continental climate zone is somewhat under-represented in the GRDC dataset due to the low
666 measurement densities over Russia, although it is well represented in the U.S. So, it may be that the global
667 improvements shown in Figure 3 are somewhat positively biased.

668
669 The maps of correlations (Figure 2) show the best results in Europe and North America where the
670 meteorological forcing is generally more accurate as a result of more data used in the re-analysis products
671 and higher station availability in the CRU data set. Also, monsoon-dominated basins are well simulated due
672 to the strong seasonal nature of both forcing and related discharge. The improvement of the 5 arc-minute
673 simulation over the 30 arc-minute simulation in Europe is mostly seen in the Alps and the Norwegian
674 mountains. This reflects the fact that topography and thus snow dynamics is better represented at higher
675 resolution as shown in Figure 4. The least accurate results are obtained for some of the African rivers, in
676 particular the Niger where the groundwater recession coefficients are probably over-estimated and inland
677 delta evaporation is under-estimated, for some rivers in the Rocky Mountains, which may be the result of
678 errors in snow dynamics and for continental Eastern Europe, which is most likely explained by an over-
679 estimation of the groundwater recession constants.

680
681



683 *Figure 2. Maps of correlation between simulated and observed discharge time series for 3597 GRDC discharge*
684 *stations; a. results for the 5 arc-minutes simulation; b. difference between results for 5 arc-minutes and 30 arc-*
685 *minutes simulation.*

686

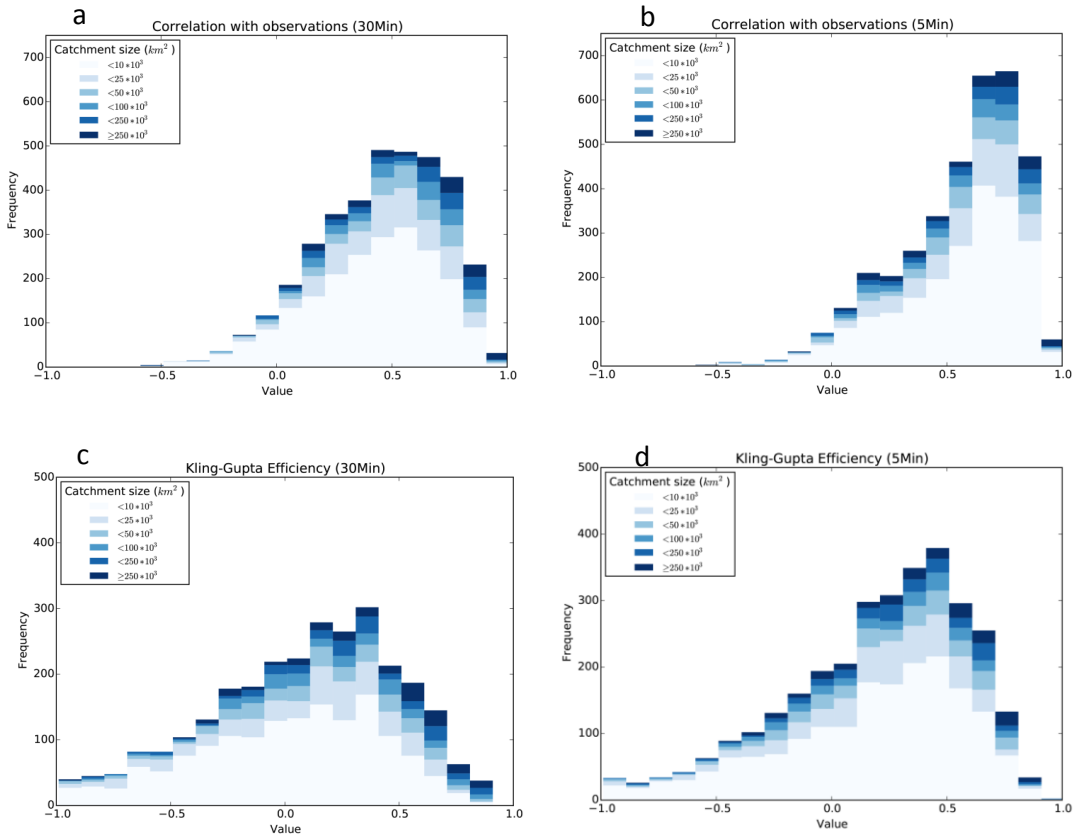
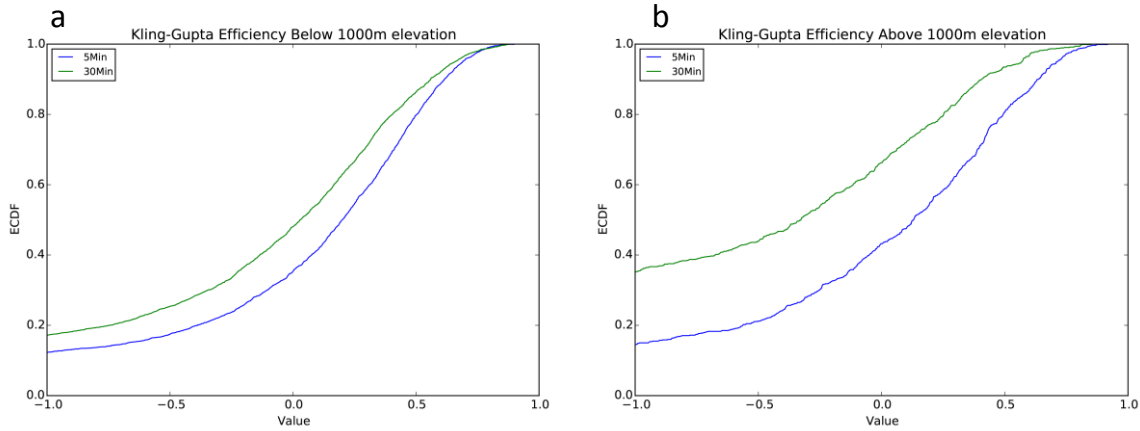


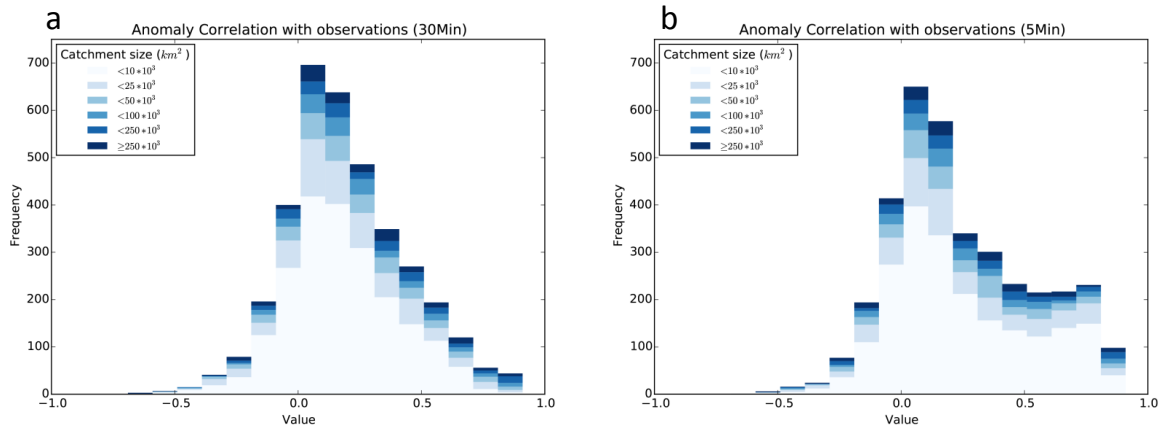
Figure 3. Histograms of evaluation statistics showing the correlation and Kling-Gupta efficiency (KGE) values for the simulated discharge for the 30 arc-minutes and the 5 arc-minute simulations based on 3597 GRDC discharge stations, a. correlation 30 arc-minute simulation, b. correlation 5 arc-minute simulation, c. KGE 30 arc-minute simulation, d. KGE 5 arc-minute simulation, note: the percentage catchments with KGE < -1 are 21% and 12% for 30 and 5 arc-minutes respectively.



695
 696 *Figure 4. Cumulative frequency distributions of Kling-Gupta efficiency (KGE) values for GRDC stations that are*
 697 *positioned below (a) and above (b) 1000 m a.m.s.l. It can be expected that for the stations above 1000 m, the*
 698 *upstream area is influenced by snow dynamics.*

699
 700 The histograms of the anomaly correlation are shown in Figure 5. The anomaly correlations are generally lower
 701 than the correlations, showing that seasonality explains part of the skill in many regions where seasonal variation is
 702 dominant when compared to intra-annual or inter-annual variability. Clearly, the 5 arc-minute results are much
 703 better than those of the half-degree simulation, indicating a higher skill with regard to capturing inter-annual
 704 anomalies. Figure 6 shows a map of the difference between the anomaly correlation and the correlation for the 5
 705 arc-minute case. This map shows that there are some regions where the anomaly correlation is better than the
 706 correlation (blue colours), e.g. snow-dominated regions in Canada and the Niger basin. These are catchments
 707 where the model has difficulty reproducing the correct seasonality as a result of errors in snow dynamics (Canada)
 708 or groundwater dynamics (Niger). Also, in case of the Niger River, not representing the inner delta flooding and
 709 resulting high evaporation may be the cause of poor seasonal timing of discharge.

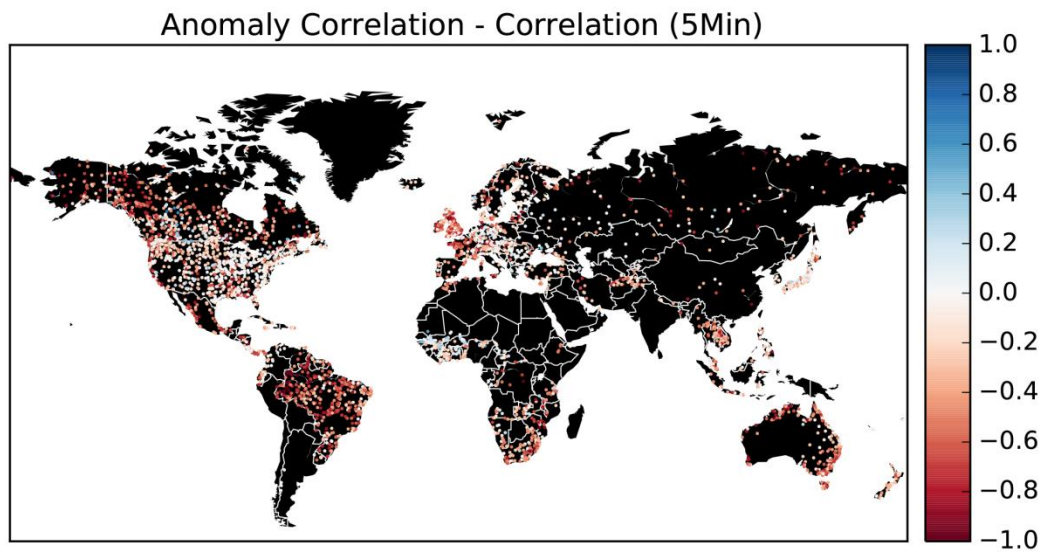
710



711

712 *Figure 5. Histograms of evaluation statistics showing the anomaly correlation for the simulated discharge for the*
 713 *30 arc-minutes and the 5 arc-minute simulations based on 3597 GRDC discharge stations, a. anomaly correlation*
 714 *half arc-degree simulation, b. anomaly correlation 5 arc-minute simulation.*

715



716

717 *Figure 6. Map showing for the 5 arc-minute run the difference between the correlation and the anomaly*
 718 *correlation between simulated and observed discharge time series for 3597 GRDC discharge stations, negative*
 719 *values mean that the correlation is higher than the anomaly correlation.*

720

721
722
723
724

3.4.2 Total water storage

725 Figure 7 compares the trends in 5 arc-minute simulated total water storage (TWS) with those from GRACE,
726 estimated as the average change in m/year over the period 2003-2015. Generally, the PCR-GLOBWB 2 simulation
727 is able to capture major groundwater depleted regions as suggested by GRACE, such as those in the Central Valley
728 aquifer, the High Plains aquifer, the North China Plain aquifer, as well as parts of the Middle East, Pakistan and
729 India. For these regions, the absolute rates of TWS change (i.e. TWS declines) of PCR-GLOBWB 2 are generally
730 larger, while the spatial pattern in the GRACE map tends to be smoother. This is mainly due to the lower
731 resolution and spatial averaging used in the GRACE product, as well as the fact that the current PCR-GLOBWB 2
732 simulation does not include lateral groundwater flow between cells. In the polar regions where GRACE estimates
733 mass loss due to melting glaciers and ice sheets, PCR-GLOBWB 2 simulates accumulation as a result of lack of a
734 glacier parameterization. Finally, there are some clear differences over the Amazon and some parts of Africa. A
735 possible explanation are errors in meteorological forcing data, which is not very accurate in these parts, but also
736 problems with the over-estimation of PCR-GLOBWB's groundwater response times in these regions which
737 therefore fail to be sufficiently sensitive to recent changes in terrestrial precipitation.

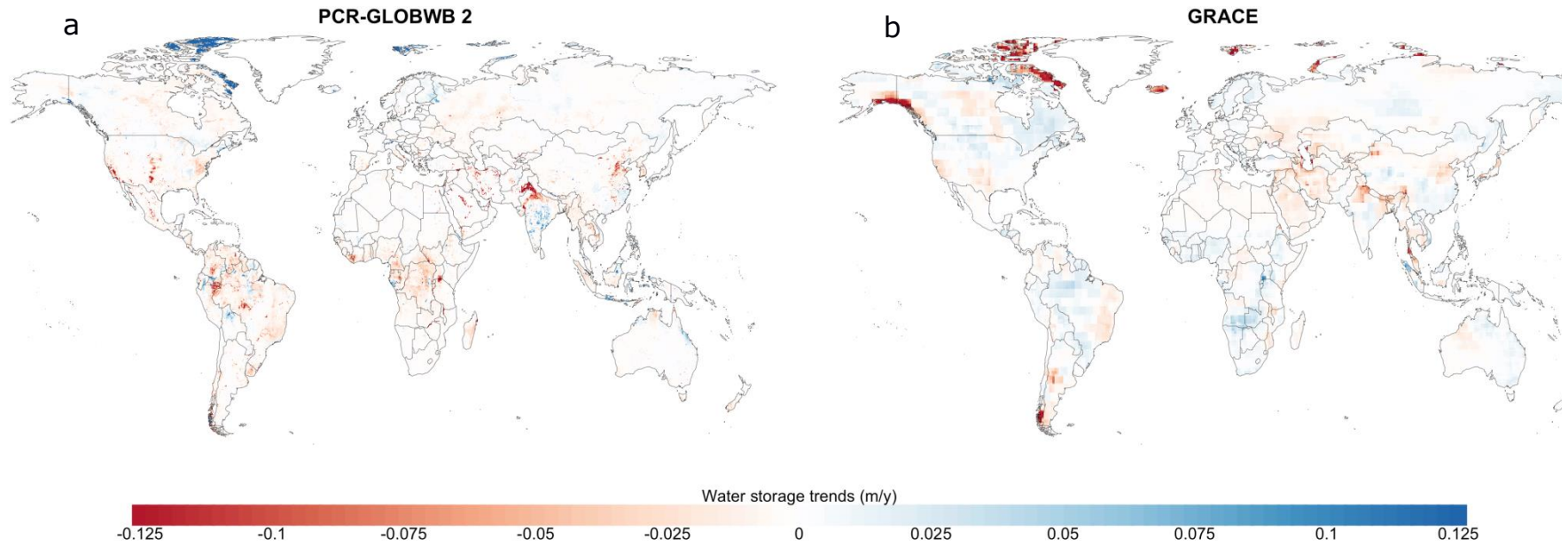
738

739 Further analyses were conducted at the basin-scale resolution, where both TWS time series of PCR-GLOBWB 2
740 and GRACE *JPL-RL05M* were averaged over a river basins areas map derived from the 5 arc-minute PCR-
741 GLOBWB drainage network. We identified all river basins with sizes larger than 900,000 km², which is similar to
742 the GRACE resolution. Smaller river basins were merged to the nearest river basins or grouped together. For the
743 remaining map of large basins, the correlations between PCR-GLOBWB 2 and GRACE basin-average monthly
744 and annual TWS time series were calculated. Monthly correlation provides information about PCR-GLOBWB's
745 ability to correctly time TWS seasonal variability (with a value equal to 1 for perfect timing), while the correlation
746 for annual time series measures inter-annual variability.

747

748 The results in Figure 8 show that PCR-GLOBWB 2 is able to capture GRACE's TWS seasonality for most basins
749 around the world, with the exception of some cold regions in high latitudes (e.g. the Yukon River basin, Iceland).
750 This shortcoming is most likely due to the lack of a proper representation of glacier and ice processes in PCR-
751 GLOBWB 2. As expected, the correlation values for inter-annual time series are generally lower than the ones for
752 monthly time series. There are some areas with negative correlation values, such as the Amazon, Niger and Nile
753 river basins. Apart from the uncertainty in the GRACE signal, these deficiencies may be related to errors in model
754 forcing and structural errors such as errors in the groundwater response time and the effects of wetlands that have
755 not been represented sufficiently well.

756



757

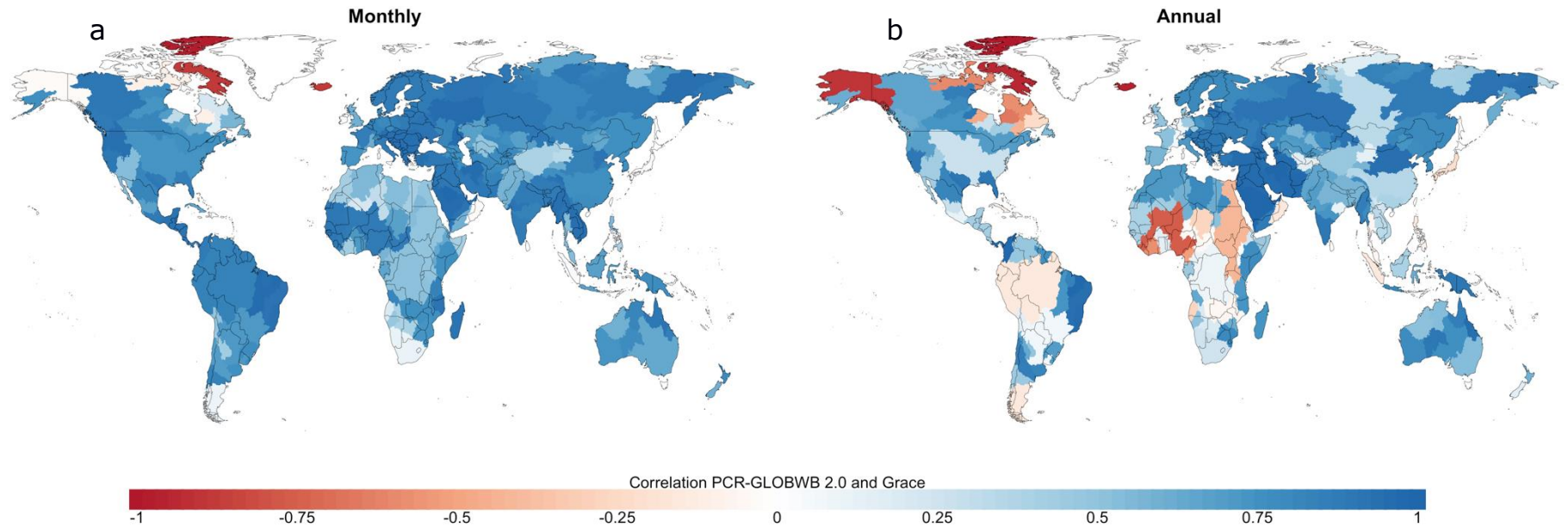
758

759

760

761

Figure 7. Comparison of PCR-GLOBWB 2 total water storage trends (m/year) with those estimated with GRACE over the period 2003-2015. a. TWS trends simulated with PCR-GLOBWB at 5 arc-minutes resolution (~10 km at the equator). Negative values indicate declining TWS (e.g. groundwater depleted regions). b. TWS trends obtained based on the GRACE JPL PL-RL05M Mascon product. The GRACE data were resampled to the resolution of 30 arc-minutes, but they actually represent the 3 x 3 arc-degree (~300 km x 300 km) area, which is the native resolution of the GRACE signal.



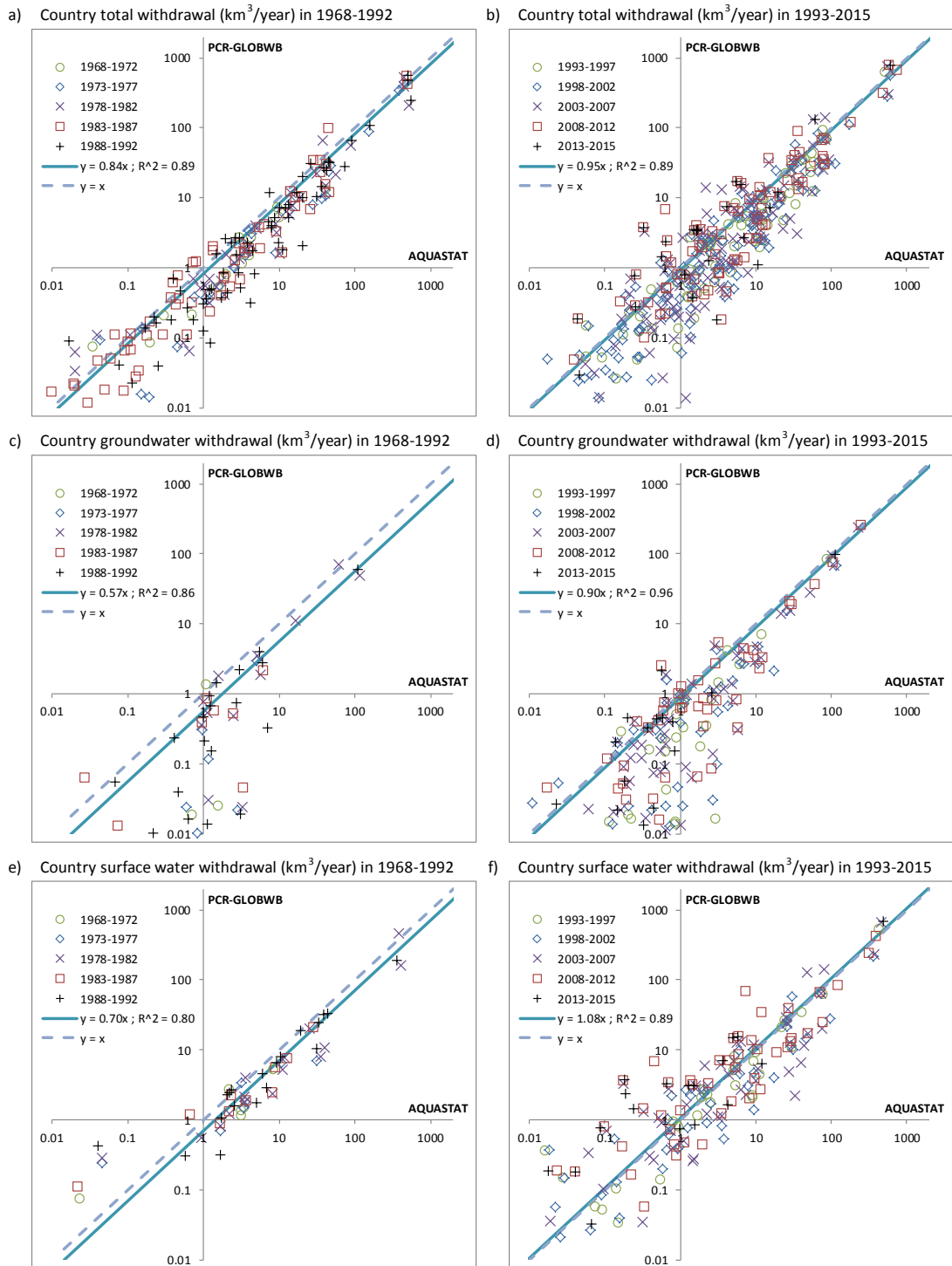
763

764

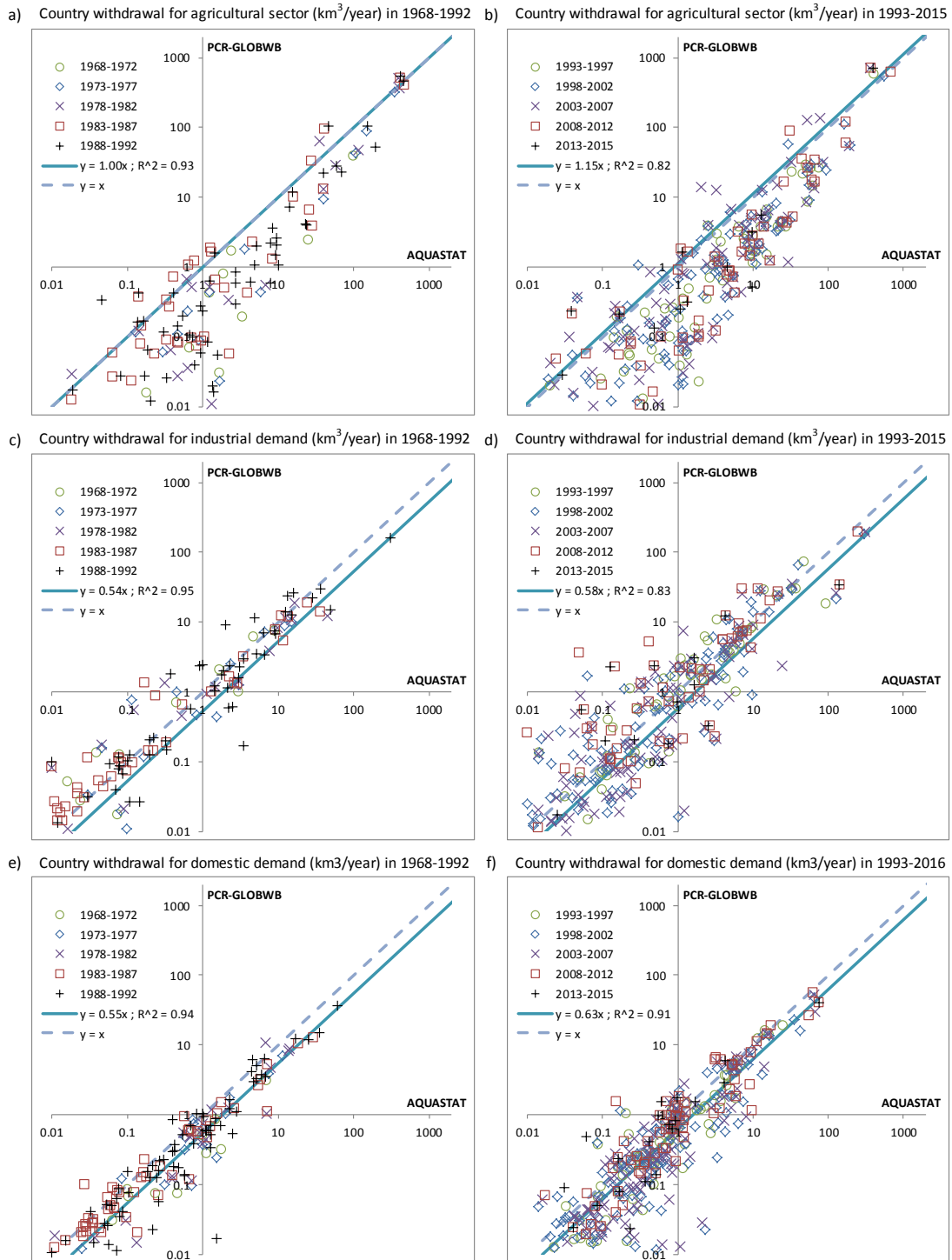
765 *Figure 8. a. Correlation between monthly TWS time series simulated PCR-GLOBWB 2 and the GRACE JPL PL-RL05M Mascon product over the period 2003-2015.*

766 *b. Comparison of annual TWS series (inter-annual variability). Comparison is only done for the larger basins over 900,000 km², conform the 3x3 arc-degree*
 767 *resolution of GRACE.*

768



769
 770 *Fig. 9: Country water withdrawal (km³/year) by source, evaluation of simulations with PCR-GLOBWB 2 with*
 771 *reported values in AQUASTAT (FAO, 2016). The scatterplots on the left (a, c, e) are for the period 1968-*
 772 *1992, while the right ones (b, d, f) are 1993-2015. The uppermost plots (a, b) are for total water withdrawal,*
 773 *the middle ones (c, d) are groundwater withdrawal, and the lowermost charts (e, f) are surface water*
 774 *withdrawal. Regression coefficient based on regression to non-log transformed data with intercept kept zero.*



775
 776 *Fig. 10: Country water withdrawal (km³/year) by sector, evaluation of simulations with PCR-GLOBWB 2 with*
 777 *reported values in AQUASTAT (FAO, 2016). The scatterplots on the left (a, c, e) are for the period 1968-*
 778 *1992, while the right ones (b, d, f) are 1993-2015. The uppermost plots (a, b) are for withdrawal for*
 779 *agricultural purpose, the middle ones (c, d) are industrial withdrawal, and the lowermost charts (e, f) are*
 780 *domestic. Regression coefficient based on regression to non-log transformed data with intercept kept zero.*

781
782
783
784
785
786
787
788
789
790
791
792
793
794
795
796
797
798
799
800
801
802
803
804
805
806
807
808
809
810
811
812
813
814

3.4.3 Water withdrawal

We compared simulated water withdrawal data from PCR-GLOBWB 2 with reported withdrawal data per country from AQUASTAT (FAO, 2016). The results are shown subdivided per source (Figure 9) and per sector (Figure 10).. Total water withdrawal and surface water withdrawal are simulated reasonably well (R^2 between 0.84 and 0.96 and regression slopes between 0.70 and 1.08). However, groundwater withdrawal is underestimated for the smaller water users. A likely explanation for this is occasional groundwater withdrawal by farmers during dry periods in areas that have not been mapped as irrigated crops in MIRCA, such as grasslands in e.g. Germany and the Netherlands, while this groundwater withdrawal is reported in AQUASTAT.

When looking at water withdrawal per sector, results are mixed. The largest agricultural water users are well captured, but the smaller ones are clearly underestimated. This is related to the fact that in many regions of the smaller water use countries, water is used for irrigation only occasionally during dry summers, while these areas are not mapped as irrigated crops in MIRCA. Also, many of these countries use irrigation technology that is not part of MIRCA, e.g. subsurface drainage by artificially high surface water levels such as in a number developed delta regions in the world. However, even though these smaller countries are not well represented, PCR-GLOBWB 2 is still able to capture the big water users, which have a significant impact on the water cycle and are most important for global scale analyses.

Both industrial and domestic water withdrawals are underestimated. The underestimation of industrial water withdrawal is partly caused by the fact that we do not include water withdrawal for thermo-electric cooling of power plants. The underestimation of domestic water withdrawal comes from the fact that we assume that the priority of water allocation is proportional to demand. This means that in times of shortage, water withdrawal is reduced with an equal percentage for agriculture, industry and domestic use. In many countries however, there is a priority series, whereby domestic demand is first met, industrial demand next and agricultural demand comes last. As a result, we underestimate domestic water withdrawal and it also partly causes the underestimation of industrial water withdrawal. This is corroborated by plotting gross water demand (which would be withdrawal if no shortage would occur) against AQUASTAT data. These plots (not shown here) result in a regression slopes of 0.68-0.75 for industrial demand and 0.78-0.92 for domestic demand. These results thus reveal that the water allocation scheme of PCR-GLOBWB 2 should be further improved.

815
816
817
818
819
820
821
822
823
824
825
826
827
828
829
830
831
832
833
834
835
836
837
838
839
840
841
842
843
844
845

4. Conclusions and future work

We presented the most recent version of the open source global hydrology and water resources model PCR-GLOBWB. This version, PCR-GLOBWB 2, has a global coverage at 5 arc-minute resolution. Apart from the higher resolution, the new model has an integrated water use scheme, i.e. every day sector specific water demand is calculated, resulting in groundwater and surface water withdrawal, water consumption and return flows. Dams and reservoirs from the GranD database (Lehner et al., 2011) are added progressively according to their year of construction. PCR-GLOBWB 2 has been rewritten in Python and uses PCRaster-Python functions (Karssenberget al., 2007). It has a modular structure, which makes the replacement and maintenance of model parts easier. PCR-GLOBWB 2 can be dynamically coupled to a global 2-layer groundwater model (de Graaf et al., 2017; Sutanudjaja et al., 2014; Sutanudjaja et al., 2011) and a one-way coupling to hydrodynamic models for large-scale inundation modelling (Hoch et al., 2017b) is also available.

Comparing the 5 arc-minute with 30 arc-minute simulations using discharge data we clearly find an improvement in the model performance of the higher resolution model. We find a general increase in correlation, anomaly correlation and KGE, indicating that the higher resolution model is better able to capture the seasonality, inter-annual anomalies and the general discharge characteristics. Also, PCR-GLOBWB 2 is able to reproduce trends and seasonality in total water storage as observed by GRACE for most river basins. It simulates the hotspots of groundwater decline that around in GRACE as well. Simulated total water withdrawal matches reasonably well with reported water withdrawal from AQUASTAT, while water withdrawal by source and sector provide mixed results.

Future work will concentrate on further improving the water withdrawal and water allocation scheme, developing a full dynamic (two-way) coupling with hydrodynamic models, developing 5 km and 1 km resolution (or higher) parameterizations of PCR-GLOBWB 2 using scale-consistent parameterizations (e.g. using MPR, Samaniego et al., 2017), incorporating a crop growth model and solving the full surface energy balance. Other foreseeable developments are using the model in probabilistic settings and in data-assimilation frameworks.

846
847
848
849
850
851
852
853
854
855
856
857
858
859
860
861
862
863
864
865
866
867
868
869
870

5. Code and data availability

PCR-GLOBWB 2 is open source and distributed under the terms of the GNU General Public License version 3, or any later version, as published by the Free Software Foundation. The model code is provided through a Github repository: https://github.com/UU-Hydro/PCR-GLOBWB_model (Sutanudjaja et al., 2017a, <https://doi.org/10.5281/zenodo.595656>). This keeps users and developers immediately aware of any new revisions. Also, it allows developers to easily collaborate, as they can download a new version, make changes, and suggest and upload the newest revisions. The configuration ini-files for the global 30 arc-minutes and 5arc-minute models and the associated model parameters and input files are provided on <https://doi.org/10.5281/zenodo.1045338> (Sutanudjaja et al., 2017b). Development and maintenance of the official version (main branch) of PCR-GLOBWB 2 is conducted at the Department of Physical Geography, Utrecht University. Yet, contributions from external parties are welcome and encouraged. For news on latest developments and papers published based on PCR-GLOBWB 2 we refer to <http://www.globalhydrology.nl> and for the underlying PCRaster-Python code to <http://pcraster.geo.uu.nl>.

Acknowledgements

We thank Utrecht University and various grants and projects that directly or indirectly contributed to the development of PCR-GLOBWB 2. The authors are very grateful to all the contributors (as acknowledged in the references) who provided the data sets used in this study. We acknowledge the Netherlands Organisation for Scientific Research (NWO) for the grant that enabled us to use the national super computer Cartesius with the help of SURFsara Amsterdam.

871 **Appendix**
872
873

Table A1 - List (non-exhaustive) of state and flux variables defined in PCR-GLOBWB

Description	Symbol	Unit
Interception storage	S_{int}	m
Snow cover/storage in water equivalent thickness (excluding liquid part S_{slq})	S_{swe}	m
Liquid/melt water storage in the snow pack	S_{slq}	m
Upper and lower soil storages	S_1 and S_2	m
Surface water storage (lakes, reservoirs, rivers and inundated water)	S_{wat}	m
groundwater storage (renewable part)	S_3	m
fossil groundwater storage (non-renewable)	S_{nrw}	m
total groundwater storage = $S_3 + S_{nrw}$	S_{gwt}	m
total water storage thickness = $S_{int} + S_{swe} + S_{slq} + S_1 + S_2 + S_{gwt}$	TWS	m
potential evaporation	E_{pot}	m.day ⁻¹
evaporation flux from the intercepted precipitation	E_{int}	m.day ⁻¹
evaporation from melt water stored in the snow pack	E_{slq}	m.day ⁻¹
bare soil evaporation	E_{soil}	m.day ⁻¹
transpiration from the upper and lower soil stores	T_1 and T_2	m.day ⁻¹
total land evaporation = $E_{pot} + E_{int} + E_{slq} + E_{soil} + T_1 + T_2$	E_{land}	m.day ⁻¹
surface water evaporation	E_{wat}	m.day ⁻¹
total evaporation = $E_{land} + E_{wat}$	E_{tot}	m.day ⁻¹
direct runoff	Q_{dr}	m.day ⁻¹
interflow, shallow sub-surface flow	Q_{sf}	m.day ⁻¹
baseflow, groundwater discharge	Q_{bf}	m.day ⁻¹
specific runoff from land	Q_{loc}	m.day ⁻¹
local change in surface water storage	Q_{wat}	m.day ⁻¹
total specific runoff	Q_{tot}	m.day ⁻¹
routed channel (surface water) discharge	Q_{chn}	m ³ .sec ⁻¹
net fluxes from the upper to lower soil stores	Q_{12}	m.day ⁻¹
net groundwater recharge, fluxes from the lower soil to groundwater stores	RCH = Q_{23}	m.day ⁻¹
surface water infiltration to groundwater	Inf	m.day ⁻¹
desalinated water withdrawal	W_{sal}	m.day ⁻¹
surface water withdrawal	W_{wat}	m.day ⁻¹
renewable groundwater withdrawal	W_3	m.day ⁻¹
non-renewable groundwater withdrawal (groundwater depletion)	W_{nrw}	m.day ⁻¹
total groundwater withdrawal = $W_3 + W_{nrw}$	W_{gwt}	m.day ⁻¹
water withdrawal allocated for irrigation purpose	A_{irr}	m.day ⁻¹
water withdrawal allocated for livestock demand/sector	A_{liv}	m.day ⁻¹
water withdrawal allocated for agricultural sector = $A_{irr} + A_{liv}$	A_{agr}	m.day ⁻¹
domestic water withdrawal	A_{dom}	m.day ⁻¹
industrial water withdrawal	A_{ind}	m.day ⁻¹

Table A2 - List of model inputs and parameters

Description	Symbol	Unit	References/sources
Upper and lower soil store parameters:			FAO (2007) soil map; van Beek and Bierkens (2009)
- Soil thickness	Z_1 and Z_2	m	
- Residual soil moisture content	θ_{r-1} and θ_{r-2}	$m^3 \cdot m^{-3}$	
- Soil moisture at saturation	θ_{s-1} and θ_{s-2}	$m^3 \cdot m^{-3}$	
- Soil water storage capacity per soil layer: $SC = Z / (\theta_s - \theta_r)$	SC_1 and SC_2	m	
- Soil matric suctions at saturation	ψ_{s-1} and ψ_{s-2}	m	
- Exponent in the soil water retention curve	β_1 and β_2	dimensionless	
- Saturated hydraulic conductivities of upper and lower soil stores	K_1 and K_2	$m \cdot day^{-1}$	
- Total soil water storage capacities = $SC_{upp} + SC_{low}$	W_{max}	m	
Land cover fraction: Land cover areas (including extent of irrigated areas) over cell areas	f_{lcov}	$m^2 \cdot m^{-2}$	GLCC v2.0 map (USGS, 1997); Olson (1994a, 1994b); MIRCA2000 dataset (Portmann et al., 2010), FAOSTAT (2012)
Topographical parameters			
- Cell-average DEM	DEM _{avg}	m	HydroSHEDS (Lehner et al., 2008); Hydro1k (Verdin and Greenlee, 1996); GTOPO30 (Gesch et al., 1999)
- Flood plain elevation	DEM _{fpl}	m	
Root fractions per soil layer	Rf_{upp} & Rf_{low}	dimensionless	Canadell et al. (1996); van Beek and Bierkens (2009)
Arno scheme (Todini, 1999; Hagemann and Gates, 2003) exponents defining soil water capacity distribution	β_{arno}	dimensionless	Canadell et al. (1996), Hagemann et al. (1999); Hagemann (2002); van Beek (2008); van Beek and Bierkens (2009)
Ratios of cell-minimum and cell-maximum soil storage to W_{max}	f_{wmin} and f_{wmax}	m	van Beek (2008); van Beek and Bierkens (2009)

Table A2 - List of model inputs and parameters (continued)

Description	Symbol	Unit	References/sources
Parameters related to phenology			
- Crop coefficient	K_c	dimensionless	Hagemann et al. (1999); Hagemann (2002); van Beek (2008); van Beek and Bierkens (2009)
- Interception capacity	$S_{int-max}$	m	
- Vegetation cover fraction	C_v	$m^2 \cdot m^{-2}$	
Groundwater parameters			
- Aquifer transmissivity	KD	$m^2 \cdot day^{-1}$	GLHYMPS map (Gleeson et al., 2014); van Beek (2008); van Beek and Bierkens (2009)
- Aquifer specific yield	S_y	$m^3 \cdot m^{-3}$	
- Groundwater recession coefficient	J	day^{-1}	
Meteorological forcing			
- Total precipitation	P	$m \cdot day^{-1}$	van Beek (2008); CRU (Harris et al., 2014); ERA40 (Uppala et al., 2005); ERA-Interim (Dee et al., 2011)
- Atmospheric air temperature	T_{air}	$^{\circ}C$ or K	
- Reference potential evaporation and transpiration	$E_{ref,pot}$	$m \cdot day^{-1}$	
Others:			
- Non-irrigation sectoral water demand (i.e. livestock, domestic and industrial)		$m \cdot day^{-1}$	Wada et al (2014)
- Desalinated water		$m \cdot day^{-1}$	Wada et al., (2011a); FAO (2016)
- Lakes and reservoirs			GLWD1 (Lehner and Döll, 2004); Grand (Lehner et al., 2011)

880 **References**

- 881
- 882 Alfieri, L., Burek, P. Dutra, E. Krzeminski, B. Muraro, D. Thielen, J., and Pappenberger F.: GloFAS—
883 Global ensemble streamflow forecasting and flood early warning, *Hydrology and Earth System*
884 *Science*, 17, 1161–1175, 2003.
- 885 Allen, R.G., Pereira, L.S., Raes, D., and Smith, M.: Crop evaporation: Guidelines for computing crop
886 requirements., UN-FAO, Rome, Italy, 1998.
- 887 Argent, R. M.: An overview of model integration for environmental applications—components,
888 frameworks and semantics, *Environmental Modelling & Software* 19 (3): 219–34,
889 doi:10.1016/S1364-8152(03)00150-6, 2004.
- 890 Bates, P.D., Horritt, M. S., and Fewtrell, T.J.: A simple inertial formulation of the shallow water
891 equations for efficient twodimensional flood inundation modelling, *Journal of Hydrology*, 38, 33–
892 45, 2010.
- 893 Bergström, S.: The HBV model, in: *Computer Models in Watershed Hydrology*, edited by Singh, V. P.,
894 Water Resources Publications, Highlands Ranch, CO, 1995.
- 895 Beven, K.J. and Cloke, H.L.: Comment on “Hyperresolution global land surface modeling: Meeting a
896 grand challenge for monitoring Earth’s terrestrial water” by Eric F. Wood et al., *Water Resources*
897 *Research*, 48, 2012.
- 898 Bierkens, M.F.P. and van Beek, L.P.H.: Seasonal Predictability of European Discharge: NAO and
899 Hydrological Response Time, *Journal of Hydrometeorology* 10, 953–968, 2009.
- 900 Bierkens, M.F.P., Bell, V.A., Burek, P., Chaney, N., Condon, L.E., David, C.H., de Roo, A., Döll, P.,
901 Drost, N., Famiglietti, J. S., Flörke, M., Gochis, D. J., Houser, P., Hut, R., Keune, J., Kollet, S.,
902 Maxwell, R. M., Reager, J. T., Samaniego, L., Sudicky, E., Sutanudjaja, E. H., van de Giesen, N.,
903 Winsemius, H., and Wood, E. F.: Hyper-resolution global hydrological modelling: what is next?
904 “Everywhere and locally relevant”, *Hydrological Processes*, 29, 310-320, 2014.
- 905 Bos, M.G.: Discharge measurement structures, third revised edition, ILRI Wageningen, 1989.
- 906 Bosmans, J. H. C., van Beek, L. P. H., Sutanudjaja, E. H., and Bierkens, M. F. P.: Hydrological impacts
907 of global land cover change and human water use, *Hydrol. Earth Syst. Sci.*, 21, 5603-5626,
908 <https://doi.org/10.5194/hess-21-5603-2017>, 2017.
- 909 Campbell, G. S.: A simple method for determining unsaturated conductivity from moisture retention
910 data, *Soil Science*, 117, 311–314, 1974.
- 911 Canadell, J., Jackson, R.B., Ehleringer, J.B. et al: Maximum rooting depth of vegetation types at the
912 global scale, *Oecologia*, <https://doi.org/10.1007/BF00329030>, 1996.
- 913 Candogan Yossef, N., Winsemius, H. Weerts, A. van Beek, L. P. H, and Bierkens, M.F.P.: Skill of a
914 global seasonal streamflow forecasting system, relative roles of initial conditions and
915 meteorological forcing, *Water Resources Research* 49, 4687–4699, 2013.
- 916 Castronova, A. M. and Goodal, J. L.: A generic approach for developing process-level hydrologic
917 modeling components.” *Environmental Modelling & Software* 25 (7): 819–25.
918 doi:10.1016/j.envsoft.2010.01.003, 2010.
- 919 Clapp, R. B. and Hornberger, G. M.: Empirical equations for some soil hydraulic properties, *Water*
920 *Resources Research*, 14, 601–604, 1978.
- 921 Cohen, S., Kettner, A. J., Syvitski, J. P. M., and Fekete, B. A. M.: WBMsed, a distributed global-scale
922 riverine sediment flux model: Model description and validation, *Computers in Geosciences*, 53, 80–
923 93, 2013.
- 924 Dalin, C., Wada, Y., Kastner, T., and M. J. Puma: Groundwater depletion embedded in international
925 food trade, *Nature*, 543, 700–704, 2017.
- 926 Dankers, R., Arnell, N. W., Clark, D. B., Falloon, P. D., Fekete, B. M., Gosling, S. N., Heinke, J., Kim,
927 H., Masaki, Y., Satoh, Y., Stacke, T., Wada, Y., and Wisser, D.: First look at changes in flood
928 hazard in the Inter-Sectoral Impact Model Intercomparison Project ensemble, *Proceedings of the*
929 *National Academy of Sciences*, 2013.
- 930 De Graaf, I. E. M., van Beek, L. P. H., Wada, Y., and Bierkens, M. F. P.: Dynamic attribution of global
931 water demand to surface water and groundwater resources: Effects of abstractions and return flows
932 on river discharges, *Advances in Water Resources* 64, 21–33, 2014.

933 De Graaf, I. E. M., Sutanudjaja, E. H., Van Beek, L. P. H., and Bierkens, M. F. P.: A high-resolution
934 global-scale groundwater model. *Hydrology and Earth System Sciences*, 19, 823-837, 2015.

935 De Graaf, I. E., van Beek, L.P.H., Gleeson, T., Moosdorf, N., Schmitz, O., Sutanudjaja, E. H., and
936 Bierkens, M. F. P.: A global-scale two-layer transient groundwater model: Development and
937 application to groundwater depletion. *Advances in Water Resources*, 102, 53-67, 2017.

938 Dee, D. P., Uppala, S. M., Simmons, A. J., Berrisford, P., Poli, P., Kobayashi, S., Andrae, U.,
939 Balmaseda, M. a., Balsamo, G., Bauer, P., Bechtold, P., Beljaars, a. C. M., van de Berg, L., Bidlot,
940 J., Bormann, N., Delsol, C., Dragani, R., Fuentes, M., Geer, a. J., Haimberger, L., Healy, S. B.,
941 Hersbach, H., Hólm, E. V., Isaksen, L., Kållberg, P., Köhler, M., Matricardi, M., McNally, a. P.,
942 Monge-Sanz, B. M., Morcrette, J.-J., Park, B.-K., Peubey, C., de Rosnay, P., Tavolato, C., Thépaut,
943 J.-N., and Vitart, F.: The ERA-Interim reanalysis: configuration and performance of the data
944 assimilation system, *Quarterly Journal of the Royal Meteorological Society*, 137, 553–597, 2011.

945 Dermody, B. J., van Beek, L. P. H., Meeks, E., Klein Goldewijk, K., Scheidel, W., van der Velde, Y.,
946 Bierkens, M. F. P., Wassen, M. J., and Dekker, S. C.: A virtual water network of the Roman world,
947 *Hydrology and Earth System Sciences*, 18, 5025–5040, [http://dx.doi.org/10.5194/hess-18-5025-](http://dx.doi.org/10.5194/hess-18-5025-2014)
948 2014, 2014.

949 Döll, P. and Siebert, S.: Global modeling of irrigation water requirements, *Water Resources Research*,
950 38, 8–1 – 8–10, 2002.

951 Döll, P., Kaspar, F., and Lehner, B.: A global hydrological model for deriving water availability
952 indicators: model tuning and validation, *Journal of Hydrology*, 270, 105–134, 2003.

953 Döll, P., Hoffmann-Dobrev, H., Portmann, F. T., Siebert, S., Eicker, A., Rodell, M., Strassberg, G., and
954 Scanlon, B. R.: Impact of water withdrawals from groundwater and surface water on continental
955 water storage variations, *Journal of Geodynamics*, 59–60, 143–156, 2012.

956 Döll, P., Muller Schmied, H., Schuh, Portmann, F. T. and Eicker, A.: Global-scale assessment of
957 groundwater depletion and related groundwater abstractions: Combining hydrological modeling
958 with information from well observations and GRACE satellites, *Water Resources Research*, 50,
959 2014.

960 Doorenbos, J. and Pruitt, W. O.: Crop water requirements, *Irrig. Drain. Pap. 24*, FAO, Rome, 1977.

961 Elliott, J., Deryng, D., Müller, C., Frieler, K., Konzmann, M., Gerten, D., Glotter, M., Flörke, M.,
962 Wada, Y., Best, N., Eisner, S., Fekete, B. M., Folberth, C., Foster, I., Gosling, S. N., Haddeland, I.,
963 Khabarov, N., Ludwig, F., Masaki, Y., Olin, S., Rosenzweig, C., Ruane, A. C., Satoh, Y., Schmid,
964 E., Stacke, T., Tang, Q., and Wisser, D.: Constraints and potentials of future irrigation water
965 availability on agricultural production under climate change, *Proceedings of the National Academy*
966 *of Sciences*, 111, 3239–3244, 2013.

967 Erkens, G. and Sutanudjaja, E. H.: Towards a global land subsidence map, *Proc. IAHS*, 372, 83-87,
968 <https://doi.org/10.5194/piahs-372-83-2015>, 2015.

969 Fekete, B. M. B., Vörösmarty, C. J. C., and Grabs, W.: High-resolution fields of global runoff
970 combining observed river discharge and simulated water balances, *Global Biogeochemical Cycles*,
971 16, 10–15, 2002.

972 Food and Agriculture Organization of the United Nations (FAO): Digital Soil Map of the World,
973 Version 3.6. FAO, Rome, Italy, 2007.

974 Food and Agriculture Organization of the United Nations (FAO): FAOSTAT statistics database,
975 <http://www.fao.org/faostat/en/#home>, 2012.

976 Food and Agriculture Organization of the United Nations (FAO): AQUASTAT database of water-
977 related data. Accessed on [2017-09-15] at: <http://www.fao.org/nr/water/aquastat/main/index.stm>,
978 2016.

979 Gesch, D.B., Verdin, K.L., and Greenlee, S.K.: New Land Surface Digital Elevation Model Covers the
980 Earth: *Eos, Transactions, American Geophysical Union*, v. 80, no. 6, p. 69–70, 1999.

981 Gleeson, T., Wada, Y., Bierkens, M. F. P., and van Beek, L. P. H.: Water balance of global aquifers
982 revealed by groundwater footprint, *Nature*, 488, 197–200, 2012.

983 Gleeson, T., N. Moosdorf, J. Hartmann, and L. P. H. van Beek: A glimpse beneath earth's surface:
984 GLobal HYdrogeology MaPS (GLHYMPS) of permeability and porosity, *Geophys. Res. Lett.*, 41,
985 3891–3898, doi:10.1002/2014GL059856, 2014.

986 Global Soil Data Task: Global Soil Data Products CD-ROM (IGBP-DIS), 2000.

987 Gosling, S. N. and Arnell, N.W.: Simulating current global river runoff with a global hydrological
988 model: model revisions, validation, and sensitivity analysis, *Hydrological Processes*, 25, 1129–
989 1145, 2011.

990 Gupta, H.V., Kling, H., Yilmaz, K.K., and Martinez, G.F.: Decomposition of the mean squared error
991 and NSE performance criteria: Implications for improving hydrological modelling. *Journal of*
992 *Hydrology*, 377, 80-91, 2009.

993 Haddeland, I., Heinke, J., Biemans, H., Eisner, S., Flörke, M., Hanasaki, N., Konzmann, M., Ludwig,
994 F., Masaki, Y., Schewe, J., Stacke, T., Tessler, Z. D., Wada, Y., and Wisser, D.: Global water
995 resources affected by human interventions and climate change, *Proceedings of the National*
996 *Academy of Sciences*, 111, 3251–3256, 2014.

997 Hagemann, S., Botzet, M., Dümenil, L., and Machenhauer, B.: Derivation of Global GCM Boundary
998 Conditions from 1 Km Land Use Satellite Data, Max-Planck-Institut für Meteorologie, Hamburg,
999 Germany, 1999.

1000 Hagemann, S.: An improved land surface parameter dataset for global and regional climate models,
1001 Max-Planck-Institut für Meteorologie, Hamburg, Germany,
1002 https://www.mpimet.mpg.de/fileadmin/publikationen/Reports/max_scirep_336.pdf, 2002.

1003 Hagemann, S. and Gates, L.D.: Improving a subgrid runoff parameterization scheme for climate mod-
1004 els by the use of high resolution data derived from satellite observations, *Climate Dynamics*, 21,
1005 349–359, 2003.

1006 Hagemann, S., Botzet, M., Dümenil, L., and Machenhauer, B.: Derivation of Global GCM Boundary
1007 Conditions from 1 Km Land Use Satellite Data, Max-Planck-Institut für Meteorologie, Hamburg,
1008 Germany, 1999.

1009 Hamon, W.: Computation of Direct Runoff Amounts from Storm Rainfall, *IAHS Publ.*, 63, 52–62,
1010 1963.

1011 Hanasaki, N., Kanae, S., Oki, T., Masuda, K., Motoya, K., Shirakawa, N., Shen, Y., and Tanaka, K.:
1012 An integrated model for the assessment of global water resources - Part 1: Model description and
1013 input meteorological forcing, *Hydrology and Earth System Science*, 12, 1007–1025, 2008.

1014 Hanasaki, N., S. Kanae, T. Oki, K. Masuda, K. Motoya, N. Shirakawa, Y. Shen, and K. Tanaka
1015 (2008b), An integrated model for the assessment of global water resources - Part 2: Applications
1016 and assessments, *Hydrology and Earth System Science*, 12, 1027–103.

1017 Hanasaki, N., Yoshikawa, S., Pokhrel, Y. and Kanae, S. A global hydrological simulation to specify the
1018 sources of water used by humans *Hydrology and Earth System Science*, 22, 789-817, 2018

1019 Harbaugh, A.W., Banta, E.R., Hill, M.C., and McDonald, M.G., 2000, MODFLOW-2000, the U.S.
1020 Geological Survey modular ground-water model -- User guide to modularization concepts and the
1021 Ground-Water Flow Process: U.S. Geological Survey Open-File Report 00-92, 121 p

1022 Harris, I., Jones, P., Osborn, T., and Lister, D.: Updated high-resolution grids of monthly climatic
1023 observations - the CRU TS3.10 Dataset, *International Journal of Climatology*, 34, 623–642, 2014.

1024 Hirabayashi Y., M. Roobavannan, K. Sujan, K. Lisako, Y. Dai, W. Satoshi, K. Hyungjun, and K.
1025 Shinjiro (2013), Global flood risk under climate change, *Nature Climate Change*, 3, 816–821.

1026 Hoch, J.M., Haag, Arjen, van Dam, Arthur, Winsemius, Hessel, van Beek, L.P.H. & Bierkens, M.F.P.:
1027 Assessing the impact of hydrodynamics on large-scale flood wave propagation - a case study for the
1028 Amazon Basin, *Hydrology and Earth System Science*, 21, 117-132, 2017a.

1029 Hoch, J.M., Neal, J.C., Baart, F. van Beek, L.P.H., Winsemius, H.C., Bates, P.D., and Bierkens,
1030 M.F.P.: GLOFRIM v1.0 – A globally applicable computational framework for integrated
1031 hydrological-hydrodynamic modelling. *Geoscientific Model Development*, 10, 3913-3929, 2017b.

1032 Karssenbergh, D., de Jong K., and van der Kwast, J.: Modelling landscape dynamics with Python,
1033 *International Journal of Geographical Information Science*, 21, 483-495, 2007.

1034 Karssenbergh, D., Schmitz, O., Salamon, P., de Jong, K., and Bierkens, M. F. P.: A software framework
1035 for construction of process-based stochastic spatio-temporal models and data assimilation,
1036 *Environmental Modelling & Software*, 25, 489–502, 2010.

1037 Kauffeldt, A., Wetterhall, F., Pappenberger, F., Salamon, P., and Thielen, J.: Technical review of large-
1038 scale hydrological models for implementation in operational flood forecasting schemes on
1039 continental level. *Environmental Modelling and Software*, 75, 68–76, 2016.

1040 Kernkamp, H.W.J., van Dam, A., Stelling, G.S. and de Goede, E.D.: Efficient scheme for the shallow
1041 water equations on unstructured grids with application to the Continental Shelf, *Ocean Dynamics*,
1042 61, 1175–1188, 2011.

1043 Konar, M., Hussein, Z., Hanasaki, N., Mauzerall, D. L., and Rodriguez-Iturbe, I.: Virtual water trade
1044 flows and savings under climate change, *Hydrology and Earth System Science*, 17, 3219–3234,
1045 2013.

1046 Konikow, L. F.: Contribution of global groundwater depletion since 1900 to sea-level rise, *Geophysical*
1047 *Research Letters* 38, L17401, 1-5, 2011.

1048 Kraijenhoff van de Leur, D.A.: A study of non-steady ground-water flow with special reference to the
1049 reservoir-coefficient, *De Ingenieur* 19, 87-94, 1958.

1050 Lehner, B. and Döll, P.: Development and validation of a global database of lakes, reservoirs and
1051 wetlands, *Journal of Hydrology* 296, 1–22, 2004.

1052 Lehner, B., Verdin, K., and Jarvis, A.: New global hydrography derived from spaceborne elevation
1053 data, *Eos (Washington. DC)*., 89, DOI: 10.1029/2008EO100001, 2008.

1054 Lehner, B., Reidy Liermann, C., Revenga, C., Vörösmarty, C., Fekete, B., Crouzet, P., Döll, P.,
1055 Endejan, M., Frenken, K., Magome, J., Nilsson, C., Robertson, J., Rödel, R., Sindorf, N., and
1056 Wisser, D.: High- resolution mapping of the world’s reservoirs and dams for sustainable river-flow
1057 management. *Frontiers in Ecology and the Environment*, 9 494–502, 2011.

1058 Liang, X., Lettenmaier, D. P., Wood, E. F., and Burges, S. J.: A simple hydrologically based model of
1059 land surface water and energy fluxes for general circulation models, *Journal of Geophysical*
1060 *Research*, 99, 14415–14428, 1994.

1061 Loveland, T. R., Reed, B. C., and Brown, J. F.: Development of a global land cover characteristics
1062 database and IGBP DISCover from 1 km AVHRR data, *International Journal of Remote Sensing*,
1063 21, 1303–1330, 2000.

1064 McDonald, R. I., Weber, K., Padowski, J., Flörke, M., Schneider, C., Green, P. A., Gleeson, T.
1065 Eckman, S. Lehner, B. Balk, D., Boucher, T. Grill, G. and Montgomery, M.: Water on an urban
1066 planet: Urbanization and the reach of urban water infrastructure. *Global Environmental Change*, 27,
1067 96-105, 2011.

1068 Murray, F.: On the computation of saturation vapor pressure, *IAHS Publ.*, 6, 203–204, 1967.

1069 New, M., Lister, D., Hulme, M., and Makin, I.: A high-resolution data set of surface climate over
1070 global land areas, *Climate Research*, 21, 1–25, 2002.

1071 Nijssen, B., O’Donnell, G. M., Lettenmaier, D. P., Lohmann, D., and Wood, E. F.: Predicting the
1072 Discharge of Global Rivers, *Journal of Climate*, 14, 3307–3323, 2001.

1073 Oki, T. and Kanae, S.: Global hydrological cycles and world water resources, *Science*, 313, 1068–
1074 1072, 2006.

1075 Olson, J. S.: Global ecosystem framework-definitions, Tech. rep., USGS EROS Data Center Internal
1076 Report, Sioux Falls, SD, 1994a.

1077 Olson, J. S.: Global ecosystem framework-translation strategy, Tech. rep., USGS EROS Data Center
1078 Internal Report, Sioux Falls, SD, 1994b.

1079 Pappenberger, F., Dutra, E., Wetterhall, F., and Cloke, H.L.: Deriving global flood hazard maps of
1080 fluvial floods through a physical model cascade, *Hydrology and Earth System Science*, 16, 4143–
1081 4156, 2012.

1082 Pokhrel, Y. N., Hanasaki, N., Yeh, P. J., Yamada, T. J., Kanae, S., and Oki, T.: Model estimates of sea-
1083 level change due to anthropogenic impacts on terrestrial water storage. *Nature Geoscience*, 5, 389-
1084 392, 2012.

1085 Pokhrel, Y. N., Koirala, S. Yeh, P. J.-F., Hanasaki, N., Longuevergne, L., Kanae, S., and Oki, T.:
1086 Incorporation of groundwater pumping in a global Land Surface Model with the representation of
1087 human impacts, *Water Resources Research*, 51, 2015.

1088 Portmann, F. T., Siebert, S., and Döll, P.: MIRCA2000-Global monthly irrigated and rainfed crop areas
1089 around the year 2000: A new high-resolution data set for agricultural and hydrological modeling,
1090 *Global Biogeochemical Cycles*, GB1011, 1-24, 2010.

1091 Prudhomme, C., Giuntoli, I., Robinson, E. L., Clark, D. B., Arnell, N. W., Dankers, R., Fekete, B. M.,
1092 Franssen, W., Gerten, D., Gosling, S. N., Hagemann, S., Hannah, D. M., Kim, H., Masaki, Y.,
1093 Satoh, Y., Stacke, T., Wada, Y., and Wisser, D.: Hydrological droughts in the 21st century, hotspots

1094 and uncertainties from a global multimodel ensemble experiment, *Proceedings of the National*
1095 *Academy of Sciences*, 111, 3262–3267, 2013.

1096 Rodell, M., Beaudoin, H. K., L'Ecuyer, T. S., Olson, W. S., Famiglietti, J. S., Houser, P. R., Adler,
1097 R., Bosilovich, M. G., Clayson, C. A., Chambers, D., Clark, E., Fetzer, E. J., Gao, X., Gu, G.,
1098 Hilburn, K., Huffman, G. J., Lettenmaier, D. P., Liu, W. T., Robertson, F. R., Schlosser, C. A.,
1099 Sheffield, J., Wood, E. F.: The Observed State of the Water Cycle in the Early Twenty-First
1100 Century. *Journal of Climate*, 28, 8289–8318, 2012.

1101 Rohwer J, Gerten D, Lucht W. Development of functional irrigation types for improved global crop
1102 modelling. PIK Report 104, 2007.

1103 Rost, S., Gerten, D., and Heyder, U.: Human alterations of the terrestrial water cycle through land
1104 management, *Advances in Geosciences*, 18, 43–50, 2008.

1105 Samaniego, L. Kumar, R., Thober, S., Rakovec, O., Zink, M., Wanders, N., Eisner, S., Müller
1106 Schmied, H., Sutanudjaja, E.H., Warrach-Sagi K., and Attinger, S.: Toward seamless hydrologic
1107 predictions across spatial scales, *Hydrology and Earth System Science*, 21, 4323–4346, 2017.

1108 Savenije, H. H. G.: The importance of interception and why we should delete the term evaporation
1109 from our vocabulary, *Hydrological Processes*, 18, 1507–1511, 2004.

1110 Schewe, J., Heinke, J., Gerten, D., Haddeland, I., Arnell, N. W., Clark, D. B., Dankers, R., Eisner, S.,
1111 Fekete, B. M., Colón-González, F. J., Gosling, S. N., Kim, H., Liu, X., Masaki, Y., Portmann, F. T.,
1112 Satoh, Y., Stacke, T., Tang, Q., Wada, Y., Wisser, D., Albrecht, T., Frieler, K., Piontek, F.,
1113 Warszawski, L., and Kabat, P.: Multimodel assessment of water scarcity under climate change,
1114 *Proceedings of the National Academy of Sciences*, 111, 3245–3250, 2014.

1115 Sheffield, J., Wood, E. F., and Munoz-Arriola, F.: Long-Term Regional Estimates of Evaporation for
1116 Mexico Based on Downscaled ISCCP Data, *Journal of Hydrometeorology*, 11, 253–275, 2010.

1117 Siebert, S., Döll, P., Hoogeveen, J., Faures, J.-M., Frenken, K., and Feick, S.: Development and
1118 validation of the global map of irrigation areas, *Hydrology and Earth System Science*, 9, 535–547,
1119 2005.

1120 Siebert, S. and Döll, P.: Quantifying blue and green virtual water contents in global crop production as
1121 well as potential production losses without irrigation, *Journal of Hydrology*, 384, 198–217, 2010.

1122 Siebert, S., Burke, J., Faures, J. M., Frenken, K., Hoogeveen, J., Döll, P., and Portmann, F. T.:
1123 Groundwater use for irrigation—a global inventory. *Hydrology and Earth System Sciences*, 14(10),
1124 1863–1880, 2010.

1125 Siebert, S., Henrich, V., Frenken, K., Burke, J.: Update of the Global Map of Irrigation Areas to
1126 version 5. Project report, 178 p., 2013.

1127 Sloan, P.G. and I.D. Moore: Modeling subsurface stormflow on steeply sloping forested watersheds,
1128 *Water Resources Research* 20, 1815–1822, 1984.

1129 Sperna Weiland, F. C., van Beek, L. P. H., Kwadijk, J. C. J., and Bierkens, M. F. P.: Global patterns of
1130 change in discharge regimes for 2100, *Hydrology and Earth System Science*, 16, 1047–1062, 2012.

1131 Sterling, S. M., Ducharne, A., and Polcher, J.: The impact of global land-cover change on the terrestrial
1132 water cycle, *Nature Climate Change*, 3, 385–390, 2013.

1133 Sutanudjaja, E. H., van Beek, L. P. H., de Jong, S. M., van Geer, F. C., and Bierkens, M. F. P.: Large-
1134 scale groundwater modeling using global datasets: a test case for the Rhine-Meuse basin, *Hydrology*
1135 *and Earth System Science*, 15, 2913–2935, 2011.

1136 Sutanudjaja, E. H.: The use of soil moisture remote sensing products for large-scale groundwater
1137 modeling and assessment, PhD thesis, Utrecht Univ., Netherlands, 2012.

1138 Sutanudjaja, E. H., van Beek, L. P. H., de Jong, S. M., van Geer, F. C., and Bierkens, M. F. P.:
1139 Calibrating a large-extent high-resolution coupled groundwater-land surface model using soil
1140 moisture and discharge data, *Water Resources Research*, 50, 687–705, 2014.

1141 Sutanudjaja, E.H., van Beek, Rens, Wanders, Niko, Wada, Yoshihide, Bosmans, Joyce, Drost, Niels,
1142 van der Ent, Ruud, de Graaf, Inge, Hoch, Jannis, de Jong, Kor, Karssenber, Derek, López López,
1143 Patricia, Peßenteiner, Stefanie, Schmitz, Oliver, Straatsma, Menno, Vannamettee, Ekkamol, Wisser,
1144 Dominik and Bierkens, Marc: PCR-GLOBWB_model: PCR-GLOBWB version v2.1.0_beta_1, ,
1145 doi:10.5281/zenodo.247139, 2017a.

1146 Sutanudjaja, E.H., van Beek, Rens, Wanders, Niko, Wada, Yoshihide, Bosmans, Joyce, Drost, Niels,
1147 van der Ent, Ruud, de Graaf, Inge, Hoch, Jannis, de Jong, Kor, Karssenber, Derek, López López,
1148 Patricia, Peßenteiner, Stefanie, Schmitz, Oliver, Straatsma, Menno, Vannamettee, Ekkamol, Wisser,

1149 Dominik and Bierkens, Marc: PCR-GLOBWB 2 input files version 2017_11_beta_1,
 1150 doi:10.5281/zenodo.1045339, 2017b.
 1151 The Global Runoff Data Centre (GRDC): The Global Runoff Database and River Discharge Data.
 1152 56068 Koblenz, Germany. Data were requested from <http://www.bafg.de/GRDC> and made available
 1153 for us on 17 April 2014, 2014.
 1154 Todini, E.: The ARNO rainfall-runoff model, *Journal of Hydrology*, 175, 339–382, 1996.
 1155 Uppala, S.M. et al.: The ERA-40 re-analysis, *Quarterly Journal of the Royal Meteorological Society*
 1156 131, 2961–3012, 2005.
 1157 USGS EROS Data Center: HYDRO1k Elevation Derivative Database, LP DAAC:
 1158 <http://edcdaac.usgs.gov/topo30/hydro/>, 2006.
 1159 Van Beek, L. P. H.: Forcing PCR-GLOBWB with CRU data, Tech. rep., Department of Physical
 1160 Geography, Utrecht University, Utrecht, The Netherlands,
 1161 <http://vanbeek.geo.uu.nl/suppinfo/vanbeek2008.pdf>, 2008.
 1162 Van Beek, L. P. H. and Bierkens, M. F. P.: The Global Hydrological Model PCR-GLOBWB:
 1163 Conceptualization, Parameterization and Verification, Tech. rep., Department of Physical
 1164 Geography, Utrecht University, Utrecht, The Netherlands,
 1165 <http://vanbeek.geo.uu.nl/suppinfo/vanbeekbierkens2009.pdf>, 2009.
 1166 Van Beek, L. P. H., Wada, Y., and Bierkens, M. F. P.: Global monthly water stress: 1. Water balance
 1167 and water availability, *Water Resources Research*, 47, W07 517, 2011.
 1168 Van Beek, L. P. H., Eikelboom, T., van Vliet, M. T. H. and Bierkens, M. F. P.: A physically based
 1169 model of global freshwater surface temperature, *Water Resources Research*, 48, W09530,
 1170 doi:10.1029/2012WR011819, 2012.
 1171 Van Vliet, M. T. H., Yearsley, J. R. F. Ludwig, Vögele, S., Lettenmaier, D.P. and Kabat, P.:
 1172 Vulnerability of US and European electricity supply to climate change, *Nature Climate Change*, 2,
 1173 676–681, 2012.
 1174 Verdin, K.L., and Greenlee, S.K.: Development of continental scale digital elevation models and
 1175 extraction of hydrographic features. In: *Proceedings, Third International Conference/Workshop on*
 1176 *Integrating GIS and Environmental Modeling*, Santa Fe, New Mexico, January 21-26, 1996.
 1177 National Center for Geographic Information and Analysis, Santa Barbara, California, 1996.
 1178 Vörösmarty, C. J., Leveque, C., and Revenga, C.: *Millennium Ecosystem Assessment Volume 1:*
 1179 *Conditions and Trends*, chap. 7: Freshwater ecosystems, Island Press, Washington DC, USA, 165–
 1180 207, 2005.
 1181 Wada, Y., van Beek, L. P. H., van Kempen, C. M., Reckman, J. W. T. M., Vasak, S., and Bierkens, M.
 1182 F. P.: Global depletion of groundwater resources, *Geophys. Res. Lett.*, 37, L20 402, 1-5, 2010.
 1183 Wada, Y., van Beek, L. P. H., Viviroli, D., Dürr, H. H., Weingartner, R., and Bierkens, M. F. P.: Global
 1184 monthly water stress: 2. Water demand and severity of water stress, *Water Resources Research*, 47,
 1185 W07 518, 1-17, 2011a.
 1186 Wada, Y., van Beek, L. P. H. and Bierkens, M.F.P.: Modelling global water stress of the recent past:
 1187 On the relative importance of trends in water demand and climate variability, *Hydrology and Earth*
 1188 *System Science*, 15, 3785–3808, 2011b.
 1189 Wada, Y., van Beek, L. P. H., and Bierkens, M. F. P.: Nonsustainable groundwater sustaining
 1190 irrigation: A global assessment, *Water Resources Research*, 48,1-18, 2012a.
 1191 Wada, Y., van Beek, L. P. H., Sperna Weiland, F. C., Chao, B. F., Wu, Y.-H., and Bierkens, M. F. P.:
 1192 Past and future contribution of global groundwater depletion to sea-level rise, *Geophysical Research*
 1193 *Letters*, 39, L09402, 1-6, 2012b.
 1194 Wada, Y., van Beek, L.P.H., Wanders N., and Bierkens, M.F.P.: Human water consumption intensifies
 1195 hydrological drought worldwide. *Environmental Research Letters* 8, 034036, 2013.
 1196 Wada, Y., Wissler, D., and Bierkens, M. F. P.: Global modeling of withdrawal, allocation and
 1197 consumptive use of surface water and groundwater resources, *Earth System Dynamics*, 5, 15–40,
 1198 2014.
 1199 Wada, Y., and M. F. P. Bierkens: Sustainability of global water use: past reconstruction and future
 1200 projections, *Environmental. Research Letters*, 9, 104003, 2014.
 1201 Wada, Y., de Graaf, I.E.M., and van Beek, L.P.H.: High-resolution modeling of human and climate
 1202 impacts on global water resources, *Journal of Advances in Modeling Earth Systems*, 8, 735–763,
 1203 2016.

1204 Wanders, N., Wada, Y., and Van Lanen, H. A. J.: Global hydrological droughts in the 21st century
1205 under a changing hydrological regime. *Earth System Dynamics*, 6, 1–15, 2015

1206 Wanders, N. and Wada, Y.: Decadal predictability of river discharge with climate oscillations over the
1207 20th and early 21st century, *Geophysical Research Letters*, 42, 10689-10695, 2015

1208 Wanders, N. and Wada, Y.: Human and climate impacts on the 21st century hydrological drought.
1209 *Journal of Hydrology*, 526, 208-220, 2016

1210 Ward, P. J., Jongman, B., Sperna-Weiland, F., Bouwman, A., van Beek, L. P. H., Bierkens, M. F. P.,
1211 Ligtvoet, W., and Winsemius, H.C.: Assessing flood risk at the global scale: Model setup, results,
1212 and sensitivity, *Environmental Research Letters*, 8, 044019, 2013.

1213 Watkins, M. M., Wiese, D. N., Yuan, D.-N., Boening, C. and Landerer, F.W.: Improved methods for
1214 observing Earth's time variable mass distribution with GRACE using spherical cap mascons,
1215 *Journal of Geophysical Research - Solid Earth*, 120, 2648–2671, 2015.

1216 Wesseling, C. G., Karssenberg, D., van Deursen, W. P. A., and Burrough, P. A.: Integrating dynamic
1217 environmental models in GIS: The development of a Dynamic Modelling language, *Transaction in*
1218 *GIS*, 1, 40–48, 1996.

1219 Wiese, D.N.: GRACE monthly global water mass grids NETCDF RELEASE 5.0. Ver. 5.0. PO.DAAC,
1220 CA, USA. Dataset accessed [2017-09-15] at <http://dx.doi.org/10.5067/TEMSC-OCL05>, 2015.

1221 Wiese, D. N., Landerer, F. W., and Watkins M. M.: Quantifying and reducing leakage errors in the JPL
1222 RL05M GRACE mascon solution, *Water Resources Research*, 52, 7490–7502, 2016.

1223 Winsemius, H. C., Van Beek, L. P. H., Jongman, B., Ward, P. J., and Bouwman, A.: A framework for
1224 global river flood risk assessments, *Hydrology and Earth System Science*, 17, 1871–1892, 2013.

1225 Winsemius, H. C., Aerts, J. C., van Beek, L. P., Bierkens, M. F.P., Bouwman, A., Jongman, B.,
1226 Kwadijk, J. C., Ligtvoet, W., Lucas, P. L., van Vuuren, D. P., and Ward, P.J.: Global drivers of
1227 future river flood risk, *Nature Climate Change*, 6, 381–385, 2016.

1228 Wisser, D., Fekete, B. M., Vörösmarty, C. J., and Schumann, A. H.: Reconstructing 20th century global
1229 hydrography: a contribution to the Global Terrestrial Network- Hydrology (GTN-H), *Hydrology*
1230 *and Earth System Sciences*, 14, 1–24, 2010.

1231 Wood, E. F., Roundy, J. K., Troy, T. J., van Beek, L. P. H., Bierkens, M. F. P., Blyth, E., de Roo, A.,
1232 Döll, P., Ek, M., Famiglietti, J., Gochis, D., van de Giesen, N., Houser, P., Jaffé, P. R., Kollet, S.,
1233 Lehner, B., Lettenmaier, D. P., Peters-Lidard, C., Sivapalan, M., Sheffield, J., Wade, A., and
1234 Whitehead, P.: Hyperresolution global land surface modeling: Meeting a grand challenge for
1235 monitoring Earth's terrestrial water, *Water Resources Research*, 47, W05 301, 1-10, 2011.

1236